Topologically induced pre-scrambling and dynamical detection of topological phase transitions at infinite temperature

Ceren B. Dağ,[1,*] L.-M. Duan,[2] and Kai Sun[1]

[1] *Department of Physics, University of Michigan, Ann Arbor, Michigan 48109, USA*
[2] *Center for Quantum Information, IIIS, Tsinghua University, Beijing 100084, PR China*

(Dated: September 27, 2019)

We report a numerical observation where the infinite-temperature out-of-time-order correlators (OTOCs) directly probe quantum phase transitions at zero temperature, in contrast to common intuition where low energy quantum effects are washed away by strong thermal fluctuations at high temperature. By comparing numerical simulations with exact analytic results, we find that this phenomenon has a topological origin and is highly generic, as long as the underlying system can be mapped to a 1D Majorana chain. Using the Majorana basis, we show that the infinite-temperature OTOCs probe zero-temperature quantum phases via detecting the presence of Majorana zero modes at the ends of the chain that is associated with 1D Z_2 topological order. Our results demonstrate an intriguing interplay between information scrambling and topological order, which leads to a new phenomenon in the scrambling of generic non-integrable models: topological order induced pre-scrambling, that defines a time-scale for the restricted scrambling of topologically-protected quantum information.

I. INTRODUCTION

Out-of-time-order correlators (OTOCs) have become a widely-appreciated tool to measure the correlation build-up in space and time, and hence quantitatively characterize information scrambling in interacting many-body systems [1–5]. Started off as a theoretical tool to understand quantum information in a black hole [6, 7] its impact quickly expanded to a wide variety of subjects including but not limited to: quantum chaos [8–12], many-body localization [3, 10, 13–15], quantum integrability [9, 12, 16, 17], quantum criticality [18] and recently symmetry-breaking quantum phase transitions [19, 20].

At temperature $T = 1/\beta$, an OTOC is defined as,

$$F(t) = \mathrm{Tr}\left(e^{-\beta H} W^\dagger(t) V^\dagger W(t) V\right), \tag{1}$$

where W and V are local quantum operators and H is the Hamiltonian. At infinite temperature ($T = \infty$ and $\beta = 0$), the Boltzmann weight $e^{-\beta H}$ becomes an identity operator and thus the OTOC reads

$$\begin{aligned} F(t) &= \frac{1}{M}\sum_{n=1}^{M} \left\langle \psi_n | W^\dagger(t) V^\dagger W(t) V | \psi_n \right\rangle, \\ &\approx \left\langle \psi_h | W^\dagger(t) V^\dagger W(t) V | \psi_h \right\rangle, \end{aligned} \tag{2}$$

Here we sum over a complete basis of the Hilbert space of dimension M, while in the second line, we use a random state $|\psi_h\rangle$ drawn from the Haar measure [15, 21] to approximate an infinite-temperature state in a correlation function, e.g. Eq. 1 [22–26].

The OTOC of a generic system is expected to decay to zero fast where the rate of decay carries information on the chaotic properties of the system; and saturate at zero in long time dynamics. Saturation at zero indicates that the system scrambles information completely, whereas a finite saturation value points to a restricted scrambling [27]. In this manuscript, we focus on the regime starting shortly after the (initial) decay of OTOC and lasts for a time interval of $\mathcal{T}$. It has been recently found that the OTOC saturation value at zero-temperature exhibits or-

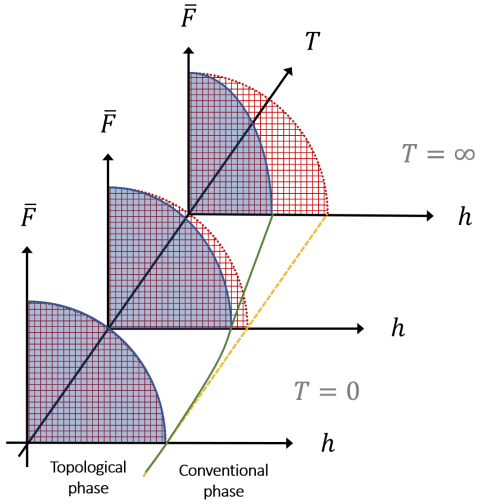

FIG. 1. The schematic of dynamic phase boundaries determined by OTOC time-average $\bar{F}$ with respect to control parameter h and temperature T. The system experiences a topological phase transition (TPT) defined at $T = 0$ temperature from Z_2 topologically ordered phase to a trivial phase. The graphics with red-grids and solid-blue show how the topological phase survives in dynamics and at higher temperatures for integrable and generic non-integrable models, respectively. While integrable models recover zero-temperature phase boundary at infinite temperature, non-integrable models experience a shift that tends to destroy order quicker than at low temperature.

* cbdag@umich.edu

der parameter-like behavior, and thus can directly probe the long-range quantum order and quantum phase transitions [19]. In contrast to the naive intuition, where thermal fluctuations wash away low energy quantum effects at high temperature, in this work we observe an emergent relation between *infinite-temperature information scrambling* and *zero-temperature Z_2 topological order* in the bulk in multiple model systems, e.g. non-interacting, interacting and/or non-integrable. The effect is robust where the qualitative features remain invariant regardless of microscopic details, e.g. integrability and symmetries. In particular, by setting W and V as local degrees of freedoms localized near the edge of the system, we find that the time-average of OTOC $\bar{F} = 1/\mathcal{T} \int dt F(t)$ (or equivalently the saturation value, if the OTOC saturates) behaves like an order parameter (Fig. 1). It is worthwhile to emphasize that the infinite temperature OTOCs are effective tools for detecting chaos that is based on the entire energy spectrum [8–12, 15]. Hence it is surprising and highly not obvious that this correlator can also directly probe zero temperature physics of the ground state, such as quantum phase transitions. *Then what is the underlying physics that allows the infinite temperature out-of-time-order correlator at the edge to accurately sense the bulk ground state physics and capture the bulk phase transition? Is this a generic feature?*

Through a careful analysis, we find that this connection arises universally as long as the quantum system can be mapped to a Majorana chain (1D superconductor) [28], and $\bar{F}$ value serves as the Z_2 topological order parameter. Furthermore our study reveals that a new time-scale appears in information scrambling when Z_2 topological order [29] exists. We name this phenomenon topologically induced pre-scrambling and hence define the time-scale as pre-scrambling time by juxtaposing the well-known phenomenon of pre-thermalization [30, 31]. Fig. 2 shows a cartoon picture of pre-scrambling for a generic (non-integrable) model with solid-red line where the system experiences restricted scrambling, $\bar{F} \neq 0$, starting at τ_{presc} for a period of time $\mathcal{T}$ after the first OTOC decay and preceding the full scrambling at τ_{sc} in a topological phase. On the other hand, the purple-dotted line in Fig. 2 shows the expected rapid OTOC decay until scrambling time τ_{sc} for a generic system with no topological order. Pre-scrambling (green) region in Fig. 2 extends to infinite-time in thermodynamic limit for systems with extensive number of symmetries, e.g. non-interacting and/or integrable limits, with no full scrambling occurring. Such systems might demonstrate $\bar{F} \neq 0$ in their trivial phases [10, 15, 32], nevertheless it is still possible to mark down the topological phase transition due to sharp transition signatures. We compare the infinite-temperature dynamic phase boundary with zero-temperature quantum phase boundary where topological order starts to develop in Fig. 1 and observe that they perfectly coincide with each other in integrable systems. Away from the integrability, the dynamical phase boundary significantly shifts away from the zero-temperature phase boundary, although the qualitative trend of $\bar{F}$ survives.

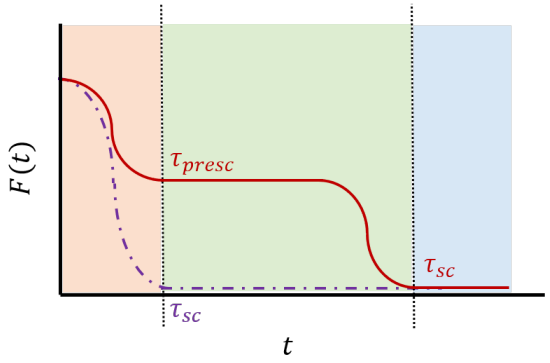

FIG. 2. The schematic of infinite-temperature OTOC evolving in time t for a quantum system with (solid-red line) and without (dotted-purple line) Z_2 topological order. A generic system with Z_2 topological order would exhibit topologically induced pre-scrambling $\bar{F} \neq 0$ before fully scrambles at scrambling time τ_{sc}. We coin τ_{presc} for the pre-scrambling time-scale. Our study focuses on this pre-scrambling regime (green panel), where the OTOC time-average exhibits order parameter like behavior (Fig. 1).

Previously, the OTOC of the integrable Ising model [16] and XX-chain [33] are analytically studied, which required periodic boundary conditions [34] and hence double-OTOCs [16, 33]. Our study indicates that OTOCs of edge operators contain new information, which is not accessible by the bulk operators. It is known that Z_2 topological order results in a two-fold degeneracy for all energy eigenstates of the entire spectrum; and recently it is pointed out that this degeneracy structure of Z_2 topological order has a highly nontrivial impact on dynamics at any temperature, e.g. long coherence times for edge spins in Ref. [35] and pre-thermalization effect in Ref. [36]. Our results extend this impact of Z_2 topological order to information scrambling and OTOCs, opens up new avenues to dynamically detect and study topological order through utilizing information scrambling as an order parameter. The dynamical detection of topological order has been under intensive investigation [35–39]. Furthermore, the topological insulators and superconductors have been studied [40–44] and classified [45] according to their non-equilibrium dynamics rather in an analogy to the classification tables for topological states of matter [46] superposed with the notion of dynamical quantum phase transitions [47–49]. Thus, understanding if the information scrambling has fundamental restrictions when topological order exists is a puzzle left at the intersection of many sub-fields.

In Sec. II, we are going to detail our numerical observation around its corresponding Majorana chain and discuss about the connection between infinite temperature scrambling and $T = 0$ topological order with quantitative arguments. Later in Sec. III, we are going to show how the topological order is encoded in the sat-

uration regime of OTOCs based on the non-interacting limit analytical calculations. In Sec. IV, we extend the discussion to interacting and/or non-integrable models and show how topological order persists in two separate contributions to the coherence times of the edge spins. Later we end Sec. IV with a discussion on topologically induced pre-scrambling in generic models and the effect of pre-scrambling on dynamic phase diagrams. We conclude in Sec. V and elaborate on possible questions to answer in the future.

II. DEMONSTRATION OF TOPOLOGICAL ORIGIN

It turns out that the connection between infinite-temperature information scrambling and quantum phases at zero temperature has a robust topological origin. Let us demonstrate how the topological origin reveals itself in the dynamics of OTOCs with an example on 1D XXZ chain,

$$H = J\sum_i \left(\sigma_i^x\sigma_{i+1}^x + \sigma_i^y\sigma_{i+1}^y + \frac{J_z}{J}\sigma_i^z\sigma_{i+1}^z\right). \quad (3)$$

At $T = 0$, the model exhibits quantum phase transitions between a gapped Ising phase $|J_z| > 1$ and a critical XY-phase $|J_z| < 1$ where the spectrum is gapless [50]. We employ Haar-distributed random states $|\psi_h\rangle$ and compute $\bar{F}$ shown in Fig. 3.

If spin operators at the edge of the chain $W = V = \sigma^z_{\text{edge}}$ are utilized (blue-circles), the infinite-temperature OTOC saturation value behaves like an order parameter of the zero-temperature quantum phase transition, i.e., $\bar{F} \sim 0$ in the XY phase ($|J_z/J| < 1$) and increases monotonically as we enter the Ising phases ($|J_z/J| > 1$). In contrast, under periodic boundary conditions (yellow diamonds line) and for a bulk spin $W = V = \sigma^z_{\text{bulk}}$ (green left-pointing triangles), the OTOC no longer differentiates the two phases, and the transition point is smoothed out consistent with predictions from Ref. [19].

To demonstrate the role of topological order, we rewrite the Hamiltonian of the XXZ model in the Majorana basis. First, via the Jordan-Wigner (JW) transformation [34]

$$\begin{aligned}\sigma_i^z &= -\prod_{j<i}\left(1-2c_j^\dagger c_j\right)\left(c_i + c_i^\dagger\right), \quad (4)\\ \sigma_i^x &= 1 - 2c_i^\dagger c_i,\\ \sigma_i^y &= -i\prod_{j<i}\left(1-2c_j^\dagger c_j\right)\left(c_i - c_i^\dagger\right).\end{aligned}$$

the spin Hamiltonian is mapped to

$$H = J\sum_i \Big[\left(1-2c_i^\dagger c_i\right)\left(1-2c_{i+1}^\dagger c_{i+1}\right) - \left(c_i + c_i^\dagger\right) \times \left(c_{i+1} - c_{i+1}^\dagger\right) + \frac{J_z}{J}\left(c_i - c_i^\dagger\right)\left(c_{i+1} + c_{i+1}^\dagger\right)\Big], \quad (5)$$

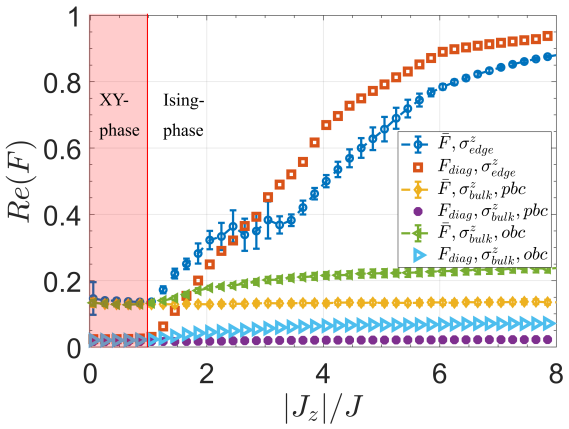

FIG. 3. Long-time average of OTOC for XXZ model for edge-spin operators $W = V = \sigma^z_{\text{edge}}$ in blue circles and its (later explained) diagonal contribution in orange squares; for bulk-spin operators σ^z_{bulk} with periodic boundary chain (pbc) in yellow diamonds and its diagonal contribution in purple hexagons; with open boundary chain (obc) in green left-pointing arrows and the diagonal contribution in light-blue right-pointing arrows. System size is $N = 14$ and the time of averaging is $tJ = 800$.

which can be written in terms of the Majorana fermions $a_{2j-1} = c_j + c_j^\dagger$ and $a_{2j} = -i\left(c_j - c_j^\dagger\right)$ [28]:

$$\begin{aligned}H = &-J\sum_i \left(a_{2i-1}a_{2i}a_{2i+1}a_{2i+2} + ia_{2i-1}a_{2i+2}\right)\\ &+ iJ_z\sum_i a_{2i}a_{2i+1}. \quad (6)\end{aligned}$$

In the Majorana basis, the spin system is mapped to an interacting Majorana chain. The XY (Ising) phase is mapped to a gapless (topological) phase, and the quantum phase transition becomes a topological transition. Same as the Kitaev chain, the topological phase in Eq. (6) develops Z_2 topological order and is characterized by two Majorana zero-modes localized at the two ends of the chain [28].

The physics can be understood by considering the $J_z \gg J$ limit, where Eq. (6) converges to the Kitaev model [28] with two zero-energy Majorana modes $\gamma_1 = a_1$ and $\gamma_2 = a_{2N}$ fully decoupled from the rest of the chain. Away from the $J_z \gg J$ limit, quartic terms in the Hamiltonian introduce interactions, but the zero-energy Majorana modes at the two ends of the chain remain topologically protected for the entire topological (Ising) phase. The existence of two Majorana modes at the two ends of the chain (γ_1 and γ_2) indicates that a zero-energy non-local fermion $d = \frac{\gamma_1 + i\gamma_2}{\sqrt{2}}$ can be defined. Because of its zero-energy nature, for an eigenstate of the Hamiltonian $|\psi_0\rangle$, another degenerate state $|\psi_1\rangle = d\,|\psi_0\rangle$ must exist with an opposite fermion parity. Therefore, in the topological phase, the edge modes are responsible of the degenerate subspaces forming not only

in the ground state, but throughout the entire spectrum [28, 50]. In other words, in contrast to an conventional (Landau-type) quantum phase transition, where across the phase boundary the ground state changes from non-degenerate (the disordered phase) to degenerate (the ordered phase), Z_2 topological order has a direct impact for the degeneracy of all eigenstates in the entire energy spectrum, i.e. two-fold degeneracy for the entire spectrum. The effect has a direct impact on measurements and dynamical quantities at any temperature [35, 36] and it is in sharp contrast to a conventional phase transition that can only be detected by zooming to the ground state at low-temperature. This is the key reason why the infinite-temperature OTOC is capable of detecting a zero-temperature topological order, but not a regular Landau-type quantum order (unless it can be mapped into a topological order).

III. TOPOLOGICAL EDGE PHYSICS ENCODED IN THE OUT-OF-TIME-ORDER CORRELATORS

In this section, we study the non-interacting limit to provide analytical arguments in the demonstration of how infinite-temperature information scrambling of edge spins encodes the existence or absence of Majorana zero-energy modes. Later we will mark the topological phase transition point via $\bar{F}$ in this non-interacting limit.

A. Transverse-field Ising Model

We consider a non-interacting, hence analytically solvable model and directly compute the contributions of Majorana zero-modes in the infinite-temperature OTOCs with edge operators. The Hamiltonian for the transverse-field Ising model with open boundary conditions is,

$$H = -J\sum_{j=1}^{N-1}\sigma_j^z\sigma_{j+1}^z + h\sum_{j=1}^{N}\sigma_j^x. \tag{7}$$

Eq. 7 has a critical point at $h = 1$ that separates a ferromagnetic ordered phase from a disordered phase. The time-average of OTOC $\bar{F}$ with σ_1^z at $\beta = 0$ is shown with the lines with blue-circles and orange-diamonds for $N = 14$ and $N = 50$, respectively in Fig. 4a. The simulation with $N = 50$ spins is performed with matrix product states (MPS) in a t-DMRG (time-dependent density matrix renormalization group) method, (see Appendix A for details). Here the error bars stand for the extend of oscillations in time, as we time-average the real part of the OTOC signal in a time interval of $tJ = \frac{\pi}{4}10 \sim 7.85$. For an edge spin operator σ_1^z, $\bar{F}$ behaves like an order parameter, which is $\bar{F} \sim -1$ in the disordered phase ($h > J$) and increase monotonically in the ordered phase ($h < J$). On the contrary, for a bulk spin operator, σ_7^z, this feature disappears (green-triangles in Fig. 4a). This observation reflects that the physics captured by edge- and bulk-spin operators are different; a similar observation to what we presented for the XXZ model earlier. To further show how the real-time OTOC dynamics look like, we contrast time-evolving OTOC $F(t)$ of edge and bulk operators in Fig. 4b. The OTOCs of the edge spin converge to different values at large times, depending on the value of h/J, while the OTOCs of bulk spins always converge to 0 at large t, as long as $h \neq 0$. The $h = 0$ limit is trivial for information scrambling, because the spin chain turns into a classical system (i.e. a classical Ising model) without quantum fluctuations or non-trivial dynamics, and thus information cannot scramble, $F(t) = 1$.

The results above can be easily understood by using the Majorana basis, which transforms the spin Hamiltonian into a non-interacting Majorana chain

$$H = -iJ\sum_{j=1}^{N-1} a_{2j}a_{2j+1} - ih\sum_{j=1}^{N} a_{2j-1}a_{2j}, \tag{8}$$

where we used Eqs. (4). In contrast to the XXZ model discussed above, Eq. (8) only contains quadratic terms, hence non-interacting, and thus can be easily diagonalized, which enables us to compute infinite-temperature OTOC saturation values $\bar{F}$ exactly. This exact solution agrees perfectly with numerical simulations in Fig. 4a. More interestingly, as will be shown below, the analytical result exhibits that F_∞ is solely contributed by Majorana zero-energy modes, while the contributions from all other finite energy excitations fade away at large t.

B. Exact solution

We compute the OTOC of an edge spin using the Majorana basis in this section. In the Majorana basis, the OTOC of Majorana fermions can be defined as $F_{2i-1,2i-1}(t) = \mathrm{Tr}\left(a_{2i-1}(t)a_{2i-1}a_{2i-1}(t)a_{2i-1}\right)/2^N$, where we set $W = V = a_{2i-1} = c_i + c_i^\dagger$. Since it can be easily showed that the OTOC of edge Majorana fermions must be identical to the OTOC of edge spins, $\sigma_1^z = \left(c_1 + c_1^\dagger\right) = \gamma_1$ and $\sigma_N^z = \mathbb{P}\left(c_N - c_N^\dagger\right) = i\mathbb{P}\gamma_2$, where $\mathbb{P} = \prod_j^N \left(1 - 2c_j^\dagger c_j\right)$ is the parity operator, here we focus on F_{11} with $W = V = a_1$.

The Majorana-fermion OTOC $F_{2i-1,2i-1}(t)$ can be conveniently computed by utilizing the Bogoliubov-de Gennes (BdG) basis, as detailed in Appendix B. With fermion operators defined for a space of double spectrum, we write the BdG Hamiltonian and calculate $F_{2i-1,2i-1}(t)$ at site i,

$$\begin{aligned} F_{\,2i-1,2i-1}(t) = & \\ & \left[\sum_\alpha^{2N}\left(|\psi_{\alpha,i}|^2 + \psi_{\alpha,i}\psi_{\alpha,i+N}^*\right)\cos\left(E_\alpha t\right)\right]^2 \\ + & \left[\sum_\alpha^{2N}\left(|\psi_{\alpha,i+N}|^2 + \psi_{\alpha,i+N}\psi_{\alpha,i}^*\right)\cos\left(E_\alpha t\right)\right]^2 - 1. \end{aligned} \tag{9}$$

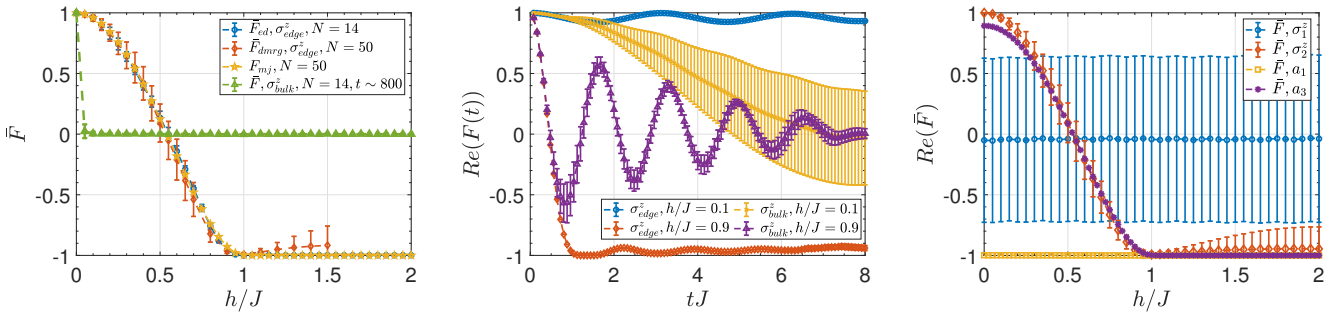

(a) (b) (c)

FIG. 4. Transverse-field Ising model at infinite-temperature. (a) The OTOC time-average of the edge spin operators σ^z_1 via real-time OTOC dynamics (blue circles) at $N = 14$ and (orange diamonds) at $N = 50$ where we used MPS (see Appendix A) for a time interval $tJ = \frac{\pi}{4}10 \sim 7.85$. The yellow-pentagrams show F_{11} based on Eq. (9) where the Majorana edge states are extracted from $H_{\rm BdG}$ matrix at $N = 50$ at infinite time limit for a comparison with other data. The green-triangles show the OTOC time-average of the bulk spin operator σ^z_7 at $N = 14$ for a time interval $tJ = \frac{\pi}{4}10^3 \sim 800$. (b) The OTOC dynamics $F(t)$ with respect to tJ. Blue-circle and orange-cross lines are the OTOC of edge σ^z_1 operator for $h = 0.1$ and $h = 0.9$, respectively. Red-diamond and purple-triangle lines are the OTOC of bulk σ^z_{25} operator for $h = 0.1$ and $h = 0.9$, respectively. All curves are computed in t-DMRG for a system size of $N = 50$, averaged over 10 random product states to generate $\beta = 0$ results. The error bars stand for 1σ variation of OTOC in this set of random states. (c) Robustness of order against changing the boundary conditions: a strong field is applied to the first spin only for $N = 13$ and $tJ \sim 8$ (blue circles); and to the edge fermions in the non-interacting fermion chain for $N = 50$ and $tJ \to \infty$ (yellow squares). The edge modes shifted to the nearest site that is free of pinning field, $\bar{F}$ of σ^z_2 spin (red-diamonds) and $\bar{F}_{33}$ of a_3 Majorana fermion (purple asterisks), respectively.

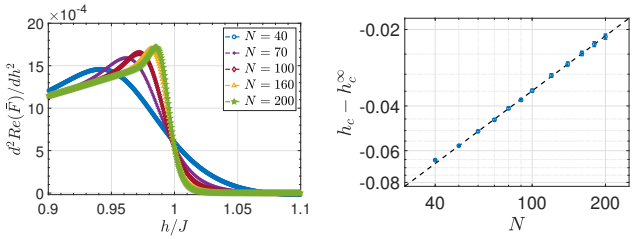

(a) (b)

FIG. 5. (a) The second derivative of the OTOC time-average $d^2\bar{F}_{11}(t \to \infty)/dh^2$ pinpoints the phase transition point via its maximum. (b) The system-size scaling of the phase transition point gives $h_{dc} \sim N^{-0.7189} + 1.0069$ with $R^2 = 0.9996$, meaning in the thermodynamic limit the OTOC pinpoints the phase transition point as $h^\infty_{dc} = 1.0069$.

where E_α and ψ_α are the eigenenergy and eigenstate of the BdG Hamiltonian, while the sum goes over all energy eigenstates $\alpha = 1, \ldots 2N$. In the long-time limit, only the non-oscillating terms (i.e., $E_\alpha = 0$) contribute to the saturation value of $F_{2i-1,2i-1}(t)$, i.e., only zero-energy modes need to be considered for $t \to \infty$. For $h < J$ in the Ising ordered phase, the BdG Hamiltonian describes a topological superconductor with Majorana zero modes at the two ends, and hence we only sum over the two Majorana zero modes, e.g. $\alpha = mj$. In the disordered phase ($h > J$), the BdG Hamiltonian describes a topologically-trivial superconductor without any zero-energy modes. Thus in the absence of zero-energy modes, $E_\alpha = 0$, $F_{2i-1,2i-1}(t) \to -1$, explaining $\bar{F}$ approaching to -1 in the Ising model results (Figs. 4). By calculating Eq. (9) as $t \to \infty$, we plot $F_{11} = F_{mj}$ in Fig. 4a with orange-pentagrams, which matches well with the Ising model results. To conclude, the derived relation, e.g. Eq. (9) rigorously proves that the saturation value of an OTOC with Majorana fermions ($W = V = a_{2i-1}$) is contributed only by Majorana zero-energy modes ($E_\alpha = 0$), while the contributions from any excited states ($E_\alpha \neq 0$) vanish at long times. Since the Ising model can be exactly mapped to a 1D Majorana chain, the infinite-temperature OTOC of the edge spins directly probes the presence or absence of the Majorana zero-energy modes. This is one of the key conclusions in our manuscript.

Motivated by this observation, we pinpoint the phase boundary of the topological phase transition in the following. Since the OTOC $F_{11}(t \to \infty)$ has a continuous transition from topologically non-trivial to trivial phase, we focus on its second derivative $d^2\bar{F}_{11}(t \to \infty)/dh^2$ with respect to external field h. The maximum of the second derivative pinpoints the transition point, Fig. 5a. Then the system-size scaling provides the transition point in the thermodynamic limit as $h^\infty_{dc} = 1.0069$ in a power-law scaling $h_{dc} \sim N^{-0.7189} + 1.0069$ (Fig. 5b). For further details, see Appendix D. We note that the results obtained in the non-interacting limit (Ising model) are valid at the infinite time in the thermodynamic limit since topologically induced pre-scrambling persists indefinitely (Appendix D).

C. Robustness against varying the boundary conditions

Although the phenomenon discussed above relies on utilizing edge degrees of freedom, all the key conclusions are robust against any local perturbations and independent of boundary conditions. Because, the physics is based on topological edge modes. To demonstrate this robustness, we vary the boundary condition of the transverse-field Ising chain by introducing a constant magnetic field (along the x direction) for the edge spin only, i.e. $h_1/J = h/J + 6$ where h_1 is the strength of the transverse field for the first site, while the rest of the spins have the same transverse field h. This strong field at the edge site introduces a strong pinning to the first spin and hence $\bar{F}$ oscillates significantly, being featureless across the phase boundary (blue-circles in Fig. 4c). However, if we choose the spin operator at the second site instead, the physics discussed above is recovered as shown in Fig. 4c with orange-diamonds. This is because such a local field cannot destroy the Majorana zero-energy mode, which is topologically protected by the nontrivial bulk. Instead, it can only move the location of the zero-energy modes, and thus, utilizing the second site, the conclusion remains the same. We additionally show the results for non-interacting fermion chain with an additive field affecting only the fermion at the edge. Yellow-squares in Fig. 4c show $\bar{F}_{mj}$ (Eq. (9)), the OTOC of edge Majorana mode γ_1 at the infinite-time limit, hence demonstrating no transition point. Purple-asterisks, on the other hand, show $\bar{F}_{33}$, the OTOC of Majorana mode a_3 at site $i = 2$ at the infinite-time limit, which is observed to match with $\bar{F}$ of the Ising model, implying an agreement between numerics and analytics.

IV. THE INTERPLAY BETWEEN TOPOLOGICAL ORDER AND SCRAMBLING

The default expectation for generic systems in 1D is scrambling over a time interval where the OTOC decays fast or slow but saturates to a residue close to zero, both depending on the set of symmetries existing in the system and the size of the Hilbert space [10, 13, 15, 32, 51]. An exception to this observation is the models that possess a symmetry-breaking phase transition with a long-range ordered phase at zero temperature regardless of the interactions [19] or the non-integrability [20]. However, could order in such generic systems be captured at higher temperatures, preferably at infinite temperature? Now we systematically study the detection of topological order in generic systems at infinite temperature.

A. Dynamical decomposition method

Since it is challenging to obtain analytical results on OTOC away from the non-interacting limit, we develop a framework that can allow us to gain more insight about detecting the topological order in generic systems via $\bar{F}$. By applying dynamical decomposition to OTOC [19], we calculate $\bar{F}$ with a term that becomes the dominant contribution in $\bar{F}$ and a correction to it, as we move away from the non-interacting limit. Dynamical decomposition method is previously utilized to find a leading-order term in $\bar{F}$ (of arbitrary bulk spins) at zero-temperature to probe zero-temperature symmetry-breaking phase transitions [19]. Here we generalize the idea to infinite temperature and put forward a conjecture in analogy to the Eigenstate Thermalization Hypothesis (ETH).

By utilizing the energy eigenstates as a complete basis of the Hilbert space, OTOC at infinite-temperature can be written as

$$F(t) = \frac{1}{M} \sum_{\alpha,\beta,\gamma,\delta} W_{\alpha\beta} V_{\beta\gamma} W_{\gamma\delta} V_{\delta\alpha} e^{i(E_\alpha - E_\beta + E_\gamma - E_\delta)t} \tag{10}$$

where $W_{\alpha\beta}$ and $V_{\alpha\beta}$ are defined as $W_{\alpha\beta} = \langle\psi_\alpha|W|\psi_\beta\rangle$ and $V_{\alpha\beta} = \langle\psi_\alpha|V|\psi_\beta\rangle$ with $|\psi_\alpha\rangle$ and $|\psi_\beta\rangle$ being the energy eigenstates with associated energies $E_\alpha, \ldots, E_\delta$. To keep the notation simpler, we do not explicitly specify the degeneracies in Eq. (10) (see Appendix C).

In the long time limit ($t \to \infty$), only the static terms with $E_\alpha - E_\beta + E_\gamma - E_\delta = 0$ contribute to the saturation value, while the rest of the terms dephase. Then the saturation value, and equivalently the long time-average $\bar{F}$, of OTOC [19] reads,

$$\bar{F} = \frac{1}{M} \left(\sum_{\substack{E_\alpha = E_\beta, \\ E_\gamma = E_\delta}} + \sum_{\substack{E_\alpha = E_\delta, \\ E_\beta = E_\gamma}} - \sum_{\substack{E_\alpha = E_\beta = \\ E_\gamma = E_\delta}} + \sum_{\substack{E_\alpha \neq E_\beta \neq \\ E_\gamma \neq E_\delta}} \right) \times W_{\alpha\beta} V_{\beta\gamma} W_{\gamma\delta} V_{\delta\alpha}, \tag{11}$$

where $\sum_{E_\alpha = E_\beta,\ E_\gamma = E_\delta}$ implies that we take the operator matrix elements that satisfy the corresponding energy condition $E_\alpha = E_\beta,\ E_\gamma = E_\delta$. Since we look for a dominant contribution to Eq. (11) as the interaction strength increases, the most suitable dynamical decomposition is through a conjecture where $\bar{F}$ is dominated by the diagonal contribution. This corresponds to the contribution with the energy condition $E_\alpha = E_\beta = E_\gamma = E_\delta$ on the spectrum. The conjecture we put forward is valid when an ansatz on the matrix elements of W and V is satisfied. This ansatz implies that the off-diagonal elements of the operator matrices are suppressed with respect to the diagonal elements when the spectrum is explicitly degenerate; and can be formulated as $|W_{E_\alpha \neq E_\beta}|^2 \ll |W_{E_\alpha = E_\beta}|^2$ for both W and V, as well as $|V_{E_\alpha \neq E_\beta}|^2 \ll |W_{E_\alpha = E_\beta}|^2$ and vice versa. When the ansatz is satisfied, $\bar{F}$ simplifies to the diagonal contribution F_{diag},

$$F_{diag} = \frac{1}{M} \sum_{\substack{E_\alpha = E_\beta = \\ E_\gamma = E_\delta}} W_{\alpha\beta} V_{\beta\gamma} W_{\gamma\delta} V_{\delta\alpha}. \tag{12}$$

If W and V are Majorana operators, i.e. a_{2i-1}, the only contribution to F_{diag} comes from the degenerate energy levels which contain two eigenstates with opposite fermion parity. Since the two-fold degeneracy arises in the entire spectrum, a finite F_{diag} is expected in the topologically non-trivial phase. However in the topologically trivial phase, although it could arise accidentally for some energy levels, two-fold degeneracy is generically not expected implying $\bar{F}_{diag} \sim 0$. Hence $\bar{F}_{diag}$ directly probes topological degeneracy in any system with Z_2 symmetry. F_{diag} can be analytically calculated in the non-interacting limit (Appendix C) via a calculation of matrix elements in edge operator W,

$$W_{\alpha\beta}\big|_{E_\alpha=E_\beta} = \langle\psi_\alpha| f(h)\gamma_1 \left(\frac{\gamma_1 + i\gamma_2}{\sqrt{2}}\right) |\psi_\alpha\rangle = \frac{2f(h)}{\sqrt{2}} = \sqrt{1-h^2}, \tag{13}$$

in the topologically non-trivial phase, $W_{\alpha\beta}\big|_{E_\alpha=E_\beta} = 0$ otherwise. Here $f(h)$ if a smooth function of magnetic field h, that can be extracted numerically for finite size systems whereas $f(h) = \sqrt{2(1-h^2)}/2$ holds in the thermodynamic limit. Hence $F_{diag} = (1-h^2)^2$ is contributed by Majorana zero-energy modes only.

We note that the operator ansatz is the generalization of ETH's second criteria [52–54] to a degenerate spectrum. However, since we do not need to assume that the diagonal elements of the operator matrix are a smooth function of energy $W_{E_\alpha=E_\beta} = g(E_\alpha)$, the first criteria of ETH [52] does not need to be followed, hence our conjecture does not require thermalization. Therefore, we can anticipate that our conjecture should be applicable for a wider range of systems e.g. including integrable but interacting systems.

As shown in the Appendix C, this conjecture can be rigorously proven for two-time correlation functions, where the off-diagonal contributions do not satisfy the corresponding energy condition $E_\alpha - E_\beta = 0$ and thus, must vanish in long time. However, for four-point correlators like OTOC, the contribution of diagonal elements is not the only way to satisfy the energy condition, and hence other contributions to $\bar{F}$ exist, e.g. off-diagonal contributions. We note that, when the operator ansatz is not satisfied, these off-diagonal contributions can become comparable to the diagonal contribution, and even can dominate $\bar{F}$. As can be supported by the numerical evidence of ETH holding in non-integrable systems [52–54], we numerically observe that the operator ansatz is satisfied away from the non-interacting limit in the Ising-type models; and hence $\bar{F}$ is dominated by diagonal contribution validating our conjecture. To demonstrate these arguments, we calculate $\bar{F}_{diag}$ for three different scenarios: i) strongly interacting but integrable case (XXZ model), ii) non-integrable models with different interacting strengths and iii) non-interacting limit.

1. *Strongly interacting but integrable case*

We revisit the Fig. 3 of the XXZ model in Sec. II. F_{diag} is shown for an edge-spin σ_1^z (obc) with red-squares; whereas the F_{diag} of bulk-spins σ_1^z (pbc) and σ_7^z (obc) operators are with purple-dots and light-blue right-pointing triangles, respectively. We observe that the diagonal contribution could be used to approximate $\bar{F}$ at the edge in the Ising phases, confirming the conjecture. Even though this model has interactions between Majorana fermions Eq. (6), it is still an integrable system which might explain why $\bar{F}$ does not completely reduce to its diagonal contribution in the long-time limit. However, the qualitative behavior is the same. The diagonal (and hence topological) contribution in the XY-phase becomes zero which is consistent with a gapless phase. Hence the sole contribution in the XY-phase is the corrections, which shows a steady non-zero residue $\bar{F} \neq 0$. This residue seems to be a consequence of the rotational symmetry of the system, $[H, S_z] = 0$ and could be expected to vanish away in the thermodynamic limit (Appendix F). Since the topological order is not visible to bulk degrees of freedom, we see $F_{diag} \sim 0$ for bulk operators.

2. *From non-integrable cases to non-interacting limit*

A generic Ising model could be introduced as,

$$H = -J\sum_{j=1}^{N-1}\sigma_j^z\sigma_{j+1}^z - \Delta\sum_{j=1}^{N-2}\sigma_j^z\sigma_{j+2}^z + h\sum_{j=1}^{N}\sigma_j^x, \tag{14}$$

$$= -iJ\sum_{j=1}^{N-1}a_{2j}a_{2j+1} + \Delta\sum_{j=1}^{N-2}a_{2i}a_{2i+1}a_{2i+2}a_{2i+3} - ih\sum_{j=1}^{N}a_{2j-1}a_{2j}, \tag{15}$$

where Δ is the next-nearest neighbor coupling between spins in Eq. 14 and breaks the integrability of the model. The strength Δ introduces interactions between Majorana fermions in Eq. 15. We focus on three different Δ values in our numerical analysis from weak to strong integrability-breaking terms (i) $\Delta/J = -0.1$, (ii) $\Delta/J = -0.5$ and (iii) $\Delta/J = -2$.

As we increase the interaction strength, $\bar{F} \sim \bar{F}_{diag}$ as expected from the conjecture. Fig. 6a compares the dynamic phase diagrams of $\Delta/J = -0.5$ and $\Delta/J = -2$ where time of averaging is fixed to $tJ = 800$ for a system size of $N = 14$. On the other hand, at the vicinity of the non-interacting limit $\Delta/J = -0.1$, $\bar{F}$ differ from its diagonal contribution $\bar{F}_{diag}$ considerably (yellow-triangles and green-circles Fig. 6b). Consistently, the operator ansatz in the non-interacting limit fails, leading to $\bar{F} \neq \bar{F}_{diag}$. Black-circles and red-diamonds in Fig. 6b show $\bar{F}$ and $\bar{F}_{diag}$ calculated at $N = 200$ in the infinite-time limit, respectively. Note that the difference is the contribution due to the off-diagonal matrix elements of

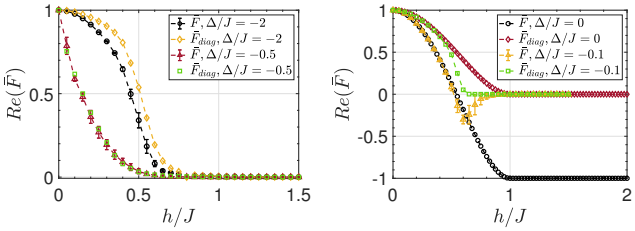

(a) (b)

FIG. 6. Comparison of $\bar{F}$ and its diagonal contribution $\bar{F}_{diag}$ at different non-integrability breaking term strength Δ/J. (a) For a time interval of $tJ = 8 \times 10^2$ and size $N = 14$, $\bar{F}$ (red-triangles) and $\bar{F}_{diag}$ (green-squares) of $\Delta/J = -0.5$; and $\bar{F}$ (black-circles) and $\bar{F}_{diag}$ (yellow-diamonds) of $\Delta/J = -2$. Hence $\bar{F} \sim \bar{F}_{diag}$ holds for a generic non-integrable system. (b) $\bar{F}$ (yellow-triangles) and $\bar{F}_{diag}$ (green-squares) of $\Delta/J = -0.1$ for a time interval of $tJ = 2 \times 10^3$ and size $N = 14$; and $\bar{F}$ (black-circles) and $\bar{F}_{diag}$ (red-diamonds) of non-interacting fermion model for a size of $N = 200$ at the infinite-time limit. At the vicinity of the non-interacting limit, off-diagonal contributions start to be significant.

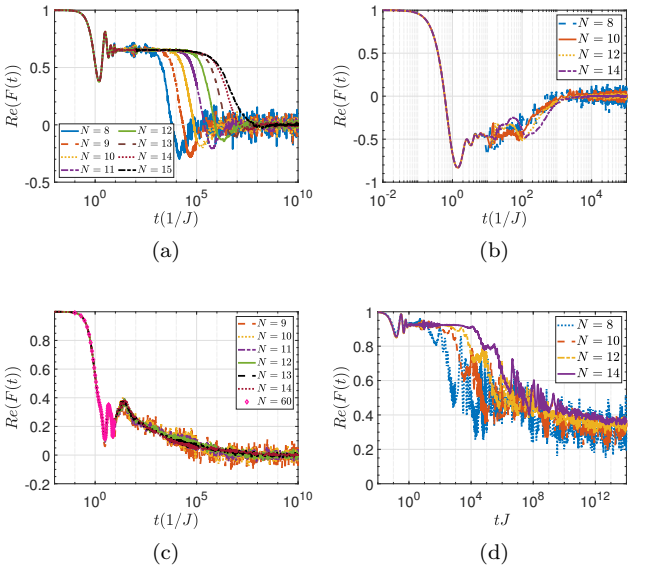

(a) (b) (c) (d)

FIG. 7. Coherence times of pre-scrambling at (a)-(b) $\Delta = -0.1$, (a) deep in the topologically non-trivial phase $h/J = 0.3$ and (b) at $h/J = 0.7$; (c) $\Delta = -0.5$ at $h/J = 0.3$ showing negative pre-scrambling values. $N = 60$ is computed via t-DMRG with 25 random initial states to have the infinite-temperature OTOC. (d) Pre-scrambling deep in the topologically non-trivial phase of XXZ model with $J_z/J = 10$ persists indefinitely.

the edge operator, which increases towards the phase boundary $h/J \to 1$ and clearly is not bounded. Remarkably off-diagonal contribution turns out to be robust, e.g. it does not vanish at infinite-time in thermodynamic limit (as seen in Fig. 6b). Robust off-diagonal contribution also shows up in a generic model at the vicinity of the non-interacting limit ($\Delta/J = -0.1$), seen in the observation that $\bar{F}$ diverges from $\bar{F}_{diag}$ (Sec. IV B and App. D). Hence we observe that OTOC (time-average) captures additional correlations that are not visible to a two-time correlator at the vicinity of the non-interacting limit. In fact, the effect of these contributions can be glimpsed at in Eq. (11) where the off-diagonal elements of the matrices explicitly contribute to $\bar{F}$. However as we move away from the special non-interacting limit, only the diagonal contribution remains topologically protected. Hence, while the conjecture does not reduce the cost of the computation, it helps us to demonstrate these additional correlations.

In the next section, we will focus on coherence times of the pre-scrambling in the non-trivial phases for generic systems and see how the pre-scrambling process governs the dynamic phase diagrams.

B. Coherence times of pre-scrambling

Z_2 topological degeneracy does not only slow down the scrambling process, but also temporarily freezes the dynamics for generic non-integrable models, causing *topologically induced pre-scrambling*. Hence we observe that the topological order has a profound effect on the dynamics of systems [35, 36], suggesting a new time-scale for information scrambling in our case. In this section, we systematically study the coherence times of the pre-scrambling process to understand its associated time-scale in the thermodynamic limit.

Fig. 7a shows how the coherence times of the weakly-interacting model ($\Delta/J = -0.1$) exponentially increase until around $N = 15$ where the increase halts, suggesting that the curves of the systems with larger sizes collapse on each other. Better examples can be seen in Figs. 7b-7c of $h/J = 0.7$ of weakly-interacting model and deep in the non-trivial phase of the model with stronger interactions $\Delta/J = -0.5$, respectively. Therefore, pre-scrambling has a finite life-time in generic systems, including the vicinity of non-interacting limit. When the model becomes integrable, pre-scrambling persists indefinitely, meaning that a system in thermodynamic limit never scrambles. Fig. 7d shows the exponential increase of pre-scrambling decay times in the XXZ model, thus implying that the observed scrambling is a finite-size effect. Similar behavior can be found for different J_z/J parameter (Appendix E), as well as the non-interacting limit (Appendix C).

We note that at which size the curve collapse would happen depends on the strength of integrability-breaking term Δ/J (interaction strength) as well as the transverse field strength h. Noting that the pre-scrambling persists indefinitely in the non-interacting limit, it is not unusual to see an initial exponential increase in N in a weakly-interacting model (Fig. 7a).

We draw attention to a main difference between Figs. 7a and 7b where the former is a point deep in

the non-trivial phase with $\bar{F} \sim \bar{F}_{diag}$ (Fig. 6b). This suggests that the coherence times of pre-scrambling in Fig. 7a mainly contributed by diagonal elements, explaining the similarity to the results in two-time correlators [35]. Whereas in Fig. 7b, we see $\bar{F}_{diag} \sim 0$, hence the OTOC time-average is mainly contributed by off-diagonal elements, which is specific to OTOC as explained in previous section. Thus, maybe most importantly the additional correlations that OTOC detects help sustaining a finite $\bar{F} \neq 0$ and contributing the pre-scrambling process.

The qualitative differences in coherence times in the topological phase is reflected to the dynamic phase diagrams (compare Figs. 7a-7c). For example, the form of decay in h/J looks different for different Δ/J: For $\Delta/J = -0.1$, we have a decay in a quadratic form $b - ah^2$ up until the dip around $h/J \sim 0.6$ and exponential afterwards (Fig. 6b), whereas for $\Delta/J = -0.5$ we see a form of exponential function in h/J only, $\sim a\exp(bh)$ (Fig. 6a). For $\Delta/J = -2$ in Fig. 6a the functional form is quadratic at $0 < h/J < 0.5$ with exponential tails in the rest of $h/J > 0.5$. The observation that topologically induced pre-scrambling occurs in a generic non-integrable system also suggests that the dynamic phase diagrams would significantly depend on the interval of the time-averaging (Appendix D for demonstration). Hence it is not clear even if a dynamical phase transition boundary could be well-defined for a generic system at infinite-temperature. We will elaborate on this intriguing question in the next section before concluding.

C. Effect of scrambling on dynamic phase diagrams

A natural question that follows the discussion in the last section is how a generic system could host pre-scrambling for mostly long but finite amount of time. Finite coherence times of edge spin two-time correlators in generic systems have been recently based on spectrum characteristics [35]. Hence these recent findings should be applicable to information scrambling. Interactions in generic spin systems tend to cause massive degeneracies in the bulk of the spectrum due to the so-called easy spin flips [35] that can happen at any site in the chain. As opposed to exponentially close and hence paired topological degeneracy due to an edge spin flip, the energies of these degenerate states are close polynomially in size. Then these massive degeneracies that increase with the system size suggest that the topological degeneracy pairing between many-body states in the thermodynamic limit becomes negligible. Therefore at infinite-temperature a generic spin system tends to scramble completely after pre-scrambling that lasts only for a finite amount of time. In other words, topological imprint of the spectrum on dynamics vanishes (no topologically-induced pre-scrambling). Additionally increasing the transverse-field strength h (linked to spin flip operator) enhances this effect on the spectrum. Hence

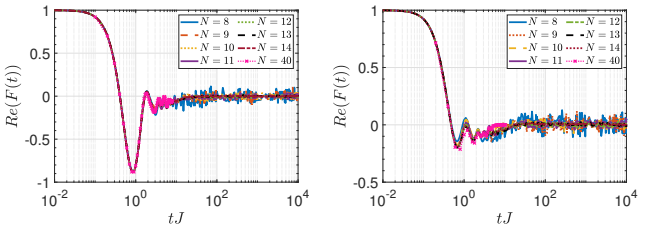

FIG. 8. Coherence times of the edge spins based on OTOC of (a) $\Delta/J = -0.5$ and (b) $\Delta/J = -2$ closer to the critical point in their respective topological phases at $h/J = 1$ for different system sizes. The size $N = 40$ in both sub-figures is calculated via t-DMRG by averaging 10 different random product states.

the full scrambling is induced early on in h before the zero temperature topological transition boundary h_c is reached. We emphasize that the zero temperature topological transition boundary h_c is governed by the ground state topological degeneracy, which is free of these so-to-speak accidental degeneracies in the rest of the spectrum.

To exemplify this argument, we bound the dynamic phase boundaries in generic systems that we study. The topological transition for $\Delta/J = -0.5$ and $\Delta/J = -2$ occurs at $h/J \sim 1.7$ and $h/J \sim 3.78$ (Appendix E), respectively. On the other hand, Fig. 6a shows early transitions for their dynamic counterparts. Since Fig. 6a is for a system size of $N = 14$, and it is yet not clear if a transition boundary could be defined purely based on pre-scrambling over a finite time interval, we aim to bound the non-trivial phase boundary instead. Figs. 8a and 8b demonstrate a very limited pre-scrambling that is mostly over in $tJ \sim 20$ for multiple system sizes that also show collapse with ED (exact diagonalization) and DMRG (density-matrix renormalization group) for $\Delta J = -0.5$ and $\Delta/J = -2$, respectively at $h/J = 1$. Hence we can safely state that the dynamic non-trivial phase boundary over a relatively long period of time is bounded to $h_{dc}/J < 1$, suggesting a significant shift from the zero-temperature phase boundaries. (h_{dc} stands for the dynamically critical h value.)

Such phase boundary shifts, though more mild than demonstrated here, in dynamical phase diagrams with corresponding symmetry-breaking transitions and that are initiated with polarized states in generic spin systems have been very recently discussed [55]. These shifts are argued to be linked to exciting the system to higher energy levels. Hence we can anticipate that working at infinite-temperature enhances the amount of shifts from the zero-temperature phase boundary. Therefore, we lower the temperature to zero and compute $\bar{F}$ and its diagonal contribution which is simply the ground state contribution $\bar{F}_{gs}$ in Fig. 9a at $N = 60$ and over a time interval of $tJ = 10$. Both $\bar{F}$ and $\bar{F}_{gs}$ behave qualitatively the same, which motivates us to apply system-size

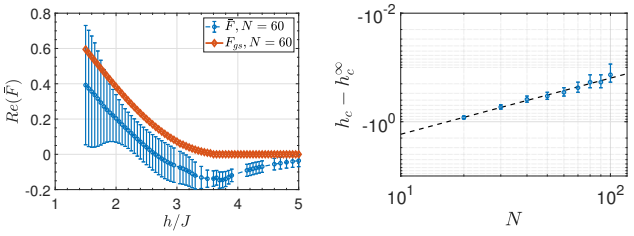

(a) (b)

FIG. 9. (a) OTOC time-average of edge spin for the non-integrable Ising model with $\Delta/J = -2$ at zero temperature and $N = 60$ system size. Blue-circles and orange-diamonds show $\bar{F}$ real-time average over $tJ = 10$ and the ground-state subspace contribution F_{gs}. (b) The system-size scaling of the critical point determined by F_{gs}. The scaling parameters read $h_{dc} \sim N^{-1.0344} + 3.8367$. All computations in (a)-(b) are done either with t-DMRG or DMRG.

scaling on $\bar{F}_{gs}$. Fig. 9b demonstrates this system-size scaling that reads $h_{dc} \sim N^{-1.0344} + 3.8367$, marking the transition point as $h_{dc}^{\infty} = 3.8367$ which is close enough to $h_c^{\infty} \sim 3.78$ (Appendix E) up to data resolution in h, $\delta_h = 0.05$. We also note that the power-law exponent extracted from $\bar{F}$ and the minimization of energy gap (Appendix E) are sufficiently close to each other, $\eta \sim -1$. Hence the dynamical phase diagram based on OTOC matches fairly well with the topological phase transition boundary in low temperature.

As a result, increasing the temperature significantly shifts the dynamic phase boundary (of OTOC) in a generic system. Whether it is possible to find a functional dependence of the h_{dc} on temperature is an interesting question that can be studied systematically in future studies.

V. CONCLUSIONS AND DISCUSSIONS

We put forward an interesting numerical observation on the XXZ model, where we showed the infinite-temperature OTOC, namely a correlator that probes the quantum chaos in interacting many-body systems, is also susceptible to ground-state phase transitions. We proved that its origin is Majorana edge modes existing in the system with a systematic study of first the non-interacting and then the generic models. We marked the topological phase transition in the non-interacting limit via $\bar{F}$. We further numerically studied the coherence times of the edge spins in the non-integrable limit and gained insight about the imprint of topological phase transitions to dynamics in the generic systems. We found that $\bar{F}$ continues to be an order parameter for the topologically non-trivial phase even in the non-integrable limit where the dynamic phase boundary is significantly altered by the temperature. Our observations on finite topological order detected via OTOC point to edge spins that remain local for long times in generic systems. Hence the scrambling of the edge spins with the rest of the system is negligible when the topological order exists. Therefore, we demonstrate how topologically-protected degrees of freedom fight against being scrambled, either completely preventing (integrable systems) or restricting (generic systems) the operator spreading and thus exhibiting a clear interplay between the topological order and scrambling. We called this process *topologically induced pre-scrambling*.

Non-integrable systems at infinite temperature are almost always expected to scramble down to zero where the decay rate depends on the symmetries existing in the Hamiltonian. However, our results indicate that this is not always the case and the scrambling can be severely hindered by the topological protection of information. This introduces the new time-scale to information scrambling, τ_{presc}. Our conclusions in principle can be generalized to higher dimensions for topological states with similar fraction excitations and topological degeneracy, although the numerical verification is yet to be found.

In principle, this probe allows experimental detection of topological states without a need to cool down the system to ultra-low temperatures whether it is the OTOCs, Eq. 12 or two-point correlators [38] when the control parameter is sufficiently away from the zero-temperature phase boundary. In particular, the infinite-temperature OTOCs are experimentally more appealing to zero-temperature OTOCs [56], since it can be challenging to prepare a ground state as the initial state in certain experimental platforms.

The interplay between information scrambling and topological order, though just started to be explored, is an intuitive one. The entanglement entropy of a ground state has a universal topological contribution in topologically non-trivial phases [57–59]. Moreover, the connection between OTOCs and the entanglement entropy of the time-evolved states has been discussed too [32, 60]. Hence here we make another connection which also relates a dynamical quantity to a static property of the Hamiltonian. As a result, $\bar{F}$ provides a robust signature to study the topological order that is independent of the perturbations and boundary conditions. Furthermore we make the role of temperature and the interval of time-averaging clear in the dynamical detection of topological phase boundaries via OTOCs in generic spin systems. While defining a dynamic phase boundary in low temperature is straightforward, it is not so as we increase the temperature. Hence, it is definitely an interesting direction how to incorporate finite temperature and thus resulting finite-time pre-scrambling effect into marking TPTs dynamically in the future.

VI. ACKNOWLEDGEMENTS

C.B.D. thanks Frank Pollmann for helpful suggestions, Chaitanya Murthy for intriguing and fruitful discussions,

and P. Myles Eugenio for helpful discussions on the manuscript and work. This work was supported by National Science Foundation under Grant EFRI-1741618.

Appendix A: Methods Explained

To determine the degeneracy in the spectrum, we need to characterize the uncertainty in energy, ΔE. This means that we define an energy window around each energy level with ΔE as $[E_m - \Delta E, E_m + \Delta E]$ where we assume that the states remain in this window are degenerate with the state whose associated energy is E_m. This process defines an energy resolution and in a way coarse-grains the energy spectrum.

As discussed in Ref. [19], the energy resolution is related to the interval of the time-evolution. Longer time-evolution translates to finer energy resolution, resolving the smallest energy differences in the spectrum, $\mathcal{T}\Delta E \sim 1$, where $\mathcal{T}$ is the total time of the evolution. Hence anytime we simulate a system with a finite time interval, we define an energy resolution as $\Delta E = \frac{\pi}{4\mathcal{T}}$. In return, the parameter ΔE determines the degenerate subspaces in the spectrum and hence helps us to determine the diagonal contribution F_{diag} in OTOC time-average. Note that this reverse relation between the time interval and energy resolution also implies that any degeneracy lifting will be eventually captured by a long-time evolution.

We call an equation derived by the dynamical decomposition as a framework equation. If the operator in the eigenbasis $W_{\alpha\beta}$ can be calculated analytically for an integrable system, that would present us the analytical expression of its OTOC saturation value. However, one can numerically derive the matrix elements $W_{\alpha\beta}$ too and use them in the framework of dynamical decomposition. Any brute force calculation of the OTOC saturation value requires an estimation on the time-dependent part in the dynamical Eq. C1, e.g. which energy pairs are equal to each other. The energy resolution ΔE is used here to define a threshold so that we could exert the degenerate subspaces on the OTOC calculation. Crudely speaking, this threshold determines whether the saturation value is contributed by the found energy set $\left\{E_{[\kappa\tau]}, E_{[\theta\alpha]}, E_{[\phi\gamma]}, E_{[\phi'\gamma']}\right\}$. In the end, the numerical incorporation of a finite energy resolution into our framework equation that analytically determines the saturation value, also provides us the time-average of OTOC over any time interval up to dramatic transient features [19]. Hence we equivalently call $\bar{F}$ both for long-time saturation value and the time-average of OTOC.

When we numerically calculate the OTOC saturation value, we do the summations in Eq. 11. This introduces an approximation to the final OTOC saturation value in our numerical result. We set a threshold where any term greater than the threshold is found and summed over. We determine our threshold based on the dimension of the Hilbert space, $\sim 1/M^2$, where M is the dimension of the Hilbert space. This generally bounds the error on the order of $\sim 10^{-2}$ (we remind the reader that $|F| \leq 1$).

We utilize ITensor platform in C++ environment and MPS (matrix product states) for our density matrix renormalization group (DMRG) computations [61]. To prepare infinite temperature states in MPS format, we average over random product states. We restrict the bond numbers to $m \lesssim 100$. Since the bond numbers increase rapidly as the system evolves in time, this results less accuracy for the later times. Therefore, we restrict our time-evolution with MPS at infinite-temperature to $tJ \lesssim 10$. The t-DMRG of OTOC in low temperatures or zero temperature present modest bond numbers, hence we are able to simulate OTOC at zero temperature for longer times.

Appendix B: Derivation of Fermionic OTOC

In order to (both analytically and numerically) solve Kitaev chain, we double the Hilbert space of single-particles and generate the BdG Hamiltonian. This Hamiltonian gives us a symmetric spectrum around energy $E = 0$ where there are two states at $E = 0$ when the chain is open due to the Majorana fermions at two ends. Therefore, if we derive an equation for OTOC in terms of single-particle states, via summing over only $E = 0$ states (Majorana zero-energy modes) due to Eq. (9), we can calculate the OTOC in the infinite-time limit.

We work with the fermion operator in doubled space, that is, in addition to $d_i = c_i$ we also have $d_{i+N} = c_i^\dagger$, hence d_i has a dimension of $2N$ where N is the dimension of the free fermionic system without pairing terms. Note that in addition to the familiar anti-commutation relation $\left\{d_i, d_j^\dagger\right\} = \delta_{ij}$, we have $\{d_i, d_{j+N}\} = \delta_{ij}$ and $\left\{d_i^\dagger, d_{j+N}^\dagger\right\} = \delta_{ij}$. Hence, a Majorana operator can be defined as $a_{2i-1} = c_i + c_i^\dagger = \left(d_i + d_i^\dagger + d_{i+N} + d_{i+N}^\dagger\right)/2$. With this algebra in mind, we can derive

$$F_{2i-1,2i-1}(t) = \frac{1}{2^N}\mathrm{Tr}\left(a_{2i-1}(t)a_{2i-1}a_{2i-1}(t)a_{2i-1}\right) \quad \text{(B1)}$$

After the substitution of d_i operators,

$$F_{2i-1,2i-1}(t) = \frac{1}{2^N}\frac{1}{2^4}\mathrm{Tr}\Big(d_i(t)a_{2i-1}d_i(t)a_{2i-1} + d_i^\dagger(t)a_{2i-1}d_i^\dagger(t)a_{2i-1} + d_{i+N}(t)a_{2i-1}d_{i+N}(t)a_{2i-1}$$
$$+ d_{i+N}^\dagger(t)a_{2i-1}d_{i+N}^\dagger(t)a_{2i-1} + 2\left(d_i(t)a_{2i-1}d_i^\dagger(t)a_{2i-1} + d_i(t)a_{2i-1}d_{i+N}(t)a_{2i-1} + d_i(t)a_{2i-1}d_{i+N}^\dagger(t)a_{2i-1}\right)$$

$$+ 2\left(d_i^\dagger(t)a_{2i-1}d_{i+N}(t)a_{2i-1} + d_i^\dagger(t)a_{2i-1}d_{i+N}^\dagger(t)a_{2i-1} + d_{i+N}^\dagger(t)a_{2i-1}d_{i+N}(t)a_{2i-1}\right)\Big). \tag{B2}$$

Since the dimension of the Hilbert space is 2^{N+1}, the following identities hold:

$$\begin{aligned}
\mathrm{Tr}\left(d_i d_i^\dagger + d_i^\dagger d_i\right) &= 2^{N+1} \rightarrow \mathrm{Tr}\left(d_i d_i^\dagger\right) = 2^N. \\
\mathrm{Tr}\left(d_{i+N} d_{i+N}^\dagger\right) &= \mathrm{Tr}\left(d_i d_{i+N}\right) \\
&= \mathrm{Tr}\left(d_i^\dagger d_{i+N}^\dagger\right) = 2^N. \\
\mathrm{Tr}\left(d_i d_i^\dagger\left(d_i^\dagger d_i + d_i d_i^\dagger\right)\right) &= 2^N \rightarrow \mathrm{Tr}\left(d_i d_i^\dagger d_i d_i^\dagger\right) = 2^N. \\
\mathrm{Tr}\left(d_{i+N} d_{i+N}^\dagger d_{i+N} d_{i+N}^\dagger\right) &= \mathrm{Tr}\left(d_i d_{i+N} d_i d_{i+N}\right) \\
&= \mathrm{Tr}\left(d_i^\dagger d_{i+N}^\dagger d_i^\dagger d_{i+N}^\dagger\right) = 2^N.
\end{aligned} \tag{B3}$$

Eq. (B2) takes a form of

$$\begin{aligned}
&F_{2i-1,2i-1}(t) = \\
&\frac{1}{2^N}\frac{1}{2^4}\sum_{k,l}^{2N}\Big[(G_{ik}(t)G_{il}(t) + G_{i+N,k}(t)G_{i+N,l}(t) \\
&+ 2G_{ik}(t)G_{i+N,l}(t))\mathrm{Tr}(d_k\gamma_i d_l\gamma_i) + \mathrm{h.c.}\Big] \\
&+ \frac{2}{2^N}\frac{1}{2^4}\sum_{k,l}^{2N}\Big[(G_{ik}(t)G_{il}^*(t) + G_{ik}(t)G_{i+N,l}^*(t)) \\
&\times \mathrm{Tr}(d_k a_{2i-1}d_l^\dagger a_{2i-1}) \\
&+ \left(G_{ik}^*(t)G_{i+N,l}(t) + G_{i+N,k}^*(t)G_{i+N,l}(t)\right) \\
&\times \mathrm{Tr}(d_k^\dagger a_{2i-1}d_l a_{2i-1})\Big],
\end{aligned} \tag{B4}$$

in terms of the matrix elements of the single-particle propagators $G(t) = \exp\left(-iH_{\mathrm{BdG}}t\right)$.

The term $\mathrm{Tr}(d_k a_{2i-1}d_l a_{2i-1})$ is non-zero only when $k = l = i$ or $k = l = i+N$ where in both cases $\mathrm{Tr}(d_k a_{2i-1}d_l a_{2i-1}) = 2^{N+2}$. The term $\mathrm{Tr}(d_k a_{2i-1}d_l^\dagger a_{2i-1})$, on the other hand, vanishes for $k = l = i$ and $k = l = i+N$, however survives for $k = l \neq i$ and $k = l \neq i+N$. In this case, $\mathrm{Tr}(d_k a_{2i-1}d_l^\dagger a_{2i-1}) = -2^{N+2}$. Note that none of these terms survives if $k = i, l = i+N$ and vice versa. Therefore we end up with

$$\begin{aligned}
F_{2i-1,2i-1}(t) = &\frac{1}{2^2}\left[(G_{ii}(t))^2 + 2\left(G_{i,i+N}(t)\right)^2 + \left(G_{i+N,i+N}(t)\right)^2 + 2\left(G_{ii}(t)G_{i+N,i}(t) + G_{i,i+N}(t)G_{i+N,i+N}(t)\right) + \mathrm{c.c}\right] \\
&- \frac{1}{2}\sum_{k\neq i,k\neq i+N}^{2N}\left(|G_{ik}(t)|^2 + |G_{i+N,k}(t)|^2 + G_{ik}(t)G_{i+N,k}^*(t) + G_{ik}^*(t)G_{i+N,k}(t)\right).
\end{aligned} \tag{B5}$$

The unitarity condition reads $\sum_k^{2N}|G_{ik}|^2 = 1$, then

$$\sum_{k\neq i,k\neq i+N}^{2N}|G_{ik}(t)|^2 = 1 - |G_{ii}(t)|^2 - |G_{i,i+N}(t)|^2 \tag{B6}$$

Furthermore, we utilize the relation $\sum_{k=1}^{2N}G_{ik}G_{i+N,k}^* = 0$ which leads to

$$\begin{aligned}
\sum_{k\neq i,k\neq i+N}^{2N}G_{ik}(t)G_{i+N,k}^*(t) = \\
-G_{ii}(t)G_{i+N,i}^*(t) - G_{i,i+N}(t)G_{i+N,i+N}^*(t).
\end{aligned} \tag{B7}$$

When these relations are utilized, one can write the final result as

$$\begin{aligned}
F_{2i-1,2i-1}(t) = &\left(\mathrm{Re}\left(G_{ii}(t)\right) + \mathrm{Re}\left(G_{i,i+N}(t)\right)\right)^2 \\
&+ \left(\mathrm{Re}\left(G_{i,i+N}(t)\right) + \mathrm{Re}\left(G_{i+N,i+N}(t)\right)\right)^2 - 1,
\end{aligned} \tag{B8}$$

for OTOC for a Majorana fermion of type a_{2i-1}. Given $G_{ij}(t) = \sum_\alpha \exp\left(-iE_\alpha t\right)\langle\psi_{\alpha,j}|\psi_{\alpha,i}\rangle$ where $\psi_{\alpha,i}$ means the i^{th} element of the eigenstate α of H_{BdG}, this result should eventually lead to the result stated in the main text,

$$\begin{aligned}
F_{2i-1,2i-1}(t) = &\left[\sum_{\alpha=1}^{2N}\left(|\psi_{i\alpha}|^2 + \psi_{i\alpha}\psi_{i+N,\alpha}^*\right)\cos\left(\epsilon_\alpha t\right)\right]^2 \\
&+ \left[\sum_{\alpha=1}^{2N}\left(|\psi_{i+N,\alpha}|^2 + \psi_{i+N,\alpha}\psi_{i,\alpha}^*\right)\cos\left(\epsilon_\alpha t\right)\right]^2 - 1.
\end{aligned} \tag{B9}$$

Appendix C: Detailed Review on Dynamical Decomposition Method and its Application to Two-time Correlators

The idea behind the dynamical decomposition method is to decompose the saturation value of a dynamical quantity over a time interval in mutually exclusive parts that might reflect different physics by either being the

leading order term or the corrections in the dynamical quantity via some assumptions [19]. For example, in Ref. [19] the assumptions are stated accordingly so that the decomposition reveals the ground state physics being the leading order term to $\bar{F}$. Therefore, we could gain insight about the relation between scrambling and symmetry-breaking phase transitions via determining how and when the OTOC could be used to dynamically detect the quantum phases. In this sense, the method helps us to see what physics is at play in a complicated dynamical correlation function, e.g. OTOC.

A correlator can be reduced to a combination of two basic constituents: eigenstate expectation values (EEV) that is the operator in the eigenbasis and the eigenstate occupation numbers (EON) that is the projection of initial state on the spectrum [52, 62, 63]. Here we will review the dynamical decomposition method by writing the degenerate structure of the spectrum explicitly. The equations in this form are used in numerical computations. We write the dynamic equation for the degenerate spectrum as,

$$\begin{aligned} F(t) = &\sum_{\theta\theta'\phi\phi'\kappa} \sum_{\alpha\beta\gamma\gamma'\tau} c^*_{[\theta\alpha]} c_{[\theta'\beta]} \\ &\times \exp\left[-i(E_{[\kappa\tau]} - E_{[\theta\alpha]} + E_{[\phi\gamma]} - E_{[\phi'\gamma']})t\right] \\ &\times W^\dagger_{[\theta\alpha][\phi\gamma]} V^\dagger_{[\phi\gamma][\phi'\gamma']} W_{[\phi'\gamma'][\kappa\tau]} V_{[\kappa\tau][\theta'\beta]}. \end{aligned} \tag{C1}$$

The initial state is $|\psi(0)\rangle = \sum_{\theta\alpha} c_{[\theta\alpha]} \left|\psi_{[\theta\alpha]}\right\rangle$, with eigenstates $\left|\psi_{[\theta\alpha]}\right\rangle$ where the symbols represent degenerate subspace θ and the state α within, respectively. Both the long-time saturation value and time-average of Eq. C1 could be obtained under the constraint $E_{[\tau\kappa]} - E_{[\theta\alpha]} + E_{[\phi\gamma]} - E_{[\phi'\gamma']} = 0$. If we focus on an infinite-temperature initial state, $[\theta\alpha] = [\theta'\beta]$ because $\mathbb{I} = |\psi_0\rangle\langle\psi_0| = \sum_{\theta\alpha} |c_{[\theta\alpha]}|^2 \left|\psi_{[\theta\alpha]}\right\rangle\left\langle\psi_{[\theta\alpha]}\right|$ and $|c_{[\theta\alpha]}|^2 = \frac{1}{M}$. In order to simplify the expression further, we assume hermitian operators and $W = V$. Then $\bar{F}$ is,

$$\begin{aligned} \bar{F} = &\sum_{\alpha\gamma\gamma'\tau} \left(\frac{2}{M} \sum_{\theta\phi} W_{[\theta\alpha][\phi\gamma]} W_{[\phi\gamma][\phi\gamma']} W_{[\phi\gamma'][\theta\tau]} W_{[\theta\tau][\theta\alpha]} - \frac{1}{M} \sum_{\theta} W_{[\theta\alpha][\theta\gamma]} W_{[\theta\gamma][\theta\gamma']} W_{[\theta\gamma'][\theta\tau]} W_{[\theta\tau][\theta\alpha]} \right) \\ &+ \sum_{\alpha\gamma\gamma'\tau} \sum_{\theta\neq\phi\neq\phi'\neq\kappa} \frac{1}{M} W_{[\theta\alpha][\phi\gamma]} W_{[\phi\gamma][\phi'\gamma']} W_{[\phi'\gamma'][\kappa\tau]} W_{[\kappa\tau][\theta\alpha]}, \end{aligned} \tag{C2}$$

in its most general form. Alongside the assumption on the initial state, (i) infinite-temperature OTOC, we apply (ii) the ansatz on the matrix elements of the operator as $|W_{[\theta\alpha][\theta'\beta]}|^2 \ll 1$ where $\theta \neq \theta'$ for the entire spectrum. This operator ansatz is more strict than the one used in Ref. [19] whose operator ansatz exerted an assumption only on the eigenstate where the phase transition is expected to happen. So, the relaxation in the initial state condition comes at a cost of making the operator condition tighter, reflecting an interesting trade-off between our two conditions.

Under the assumptions (i)-(ii), the OTOC saturation dynamically decomposes into a diagonal contribution F_{diag} and corrections (off-diagonal contribution). In the topologically non-trivial phase, the fluctuations are suppressed between the matrix elements in all subspaces, implying $|W_{[\theta\alpha][\theta\beta]}| \sim \mathcal{O}(1)$. Hence the operator ansatz in the topologically non-trivial phase takes the form $|W_{[\theta\gamma][\theta\gamma']}|^2 \gg |W_{[\theta\alpha][\theta'\beta]}|^2$, as stated in the main text. Therefore, we derive the diagonal contribution in this phase as,

$$\begin{aligned} &F_{diag} = \\ &\tfrac{1}{M} \textstyle\sum_{\theta} \sum_{\alpha\gamma\gamma'\tau} W_{[\theta\alpha][\theta\gamma]} W_{[\theta\gamma][\theta\gamma']} W_{[\theta\gamma'][\theta\tau]} W_{[\theta\tau][\theta\alpha]}. \end{aligned} \tag{C3}$$

This equation is the Eq. (12) in the main text, written in the notation that takes the degeneracy explicitly into account. The operator ansatz in the topologically non-trivial phase simultaneously guarantees that the OTOC Eq. (C2) is dominated by the diagonal contribution Eq. (C3), leading to our conjecture.

Similar to a disordered phase in a symmetry-breaking phase transition, in the topologically trivial phase the fluctuations are expected to exist between the matrix elements in any subspace, leading to the absence of order $|W_{[\theta\alpha][\theta\beta]}| \sim 0$, and hence $F_{diag} \sim 0$. Then the off-diagonal correction term dominates the OTOC, while the operator ansatz $|W_{[\theta\alpha][\theta'\beta]}|^2 \ll 1$ still guarantees bounded corrections. The importance of bounded corrections can be seen in generic models, giving rise to bounded OTOC signature in topologically trivial phases. To conclude, since (i) Eq. (C3) captures the diagonal contribution throughout the spectrum and if (ii) the corrections remain bounded due to the operator ansatz, the topological order can be dynamically detectable via OTOC time-average of an edge operator at infinite-temperature.

As already pointed out by earlier studies [35, 36, 38] in different forms, one can write the saturation value of a two-time correlator of edge Majorana fermions as

$$\begin{aligned} C_\infty &= \mathrm{Tr}\left(W(t)W\right) \\ &= \frac{1}{M} \sum_{\theta} \sum_{\alpha\gamma} W_{[\theta\alpha][\theta\gamma]} W_{[\theta\gamma][\theta\alpha]}, \end{aligned} \tag{C4}$$

at infinite temperature where $W = \sigma_1^z = \gamma_1$. Eq. (C4) shows that the saturation value of a two-time correlator will always be governed by the diagonal elements in the operator W. Then $W_{[\theta\alpha][\theta\gamma]} = \langle\psi_{[\theta\alpha]}| W |\psi_{[\theta\gamma]}\rangle$ can be straightforwardly calculated in the non-interacting limit. Here, $|\psi_{[\theta\gamma]}\rangle$ and $|\psi_{[\theta\alpha]}\rangle$ are even and odd parity states in a doubly-degenerate subspace that is dictated by the Majorana zero-energy modes. We note that $|\psi_{[\theta\gamma]}\rangle = d|\psi_{[\theta\alpha]}\rangle = f(h)\left(\frac{\gamma_1+i\gamma_2}{\sqrt{2}}\right)|\psi_{[\theta\alpha]}\rangle$, where $f(h)$ is a function of magnetic field h and $f(h=0) = 1/\sqrt{2}$, however decreases as $h \to 1$. The quantity that we need to calculate becomes $\langle\psi_{[\theta\alpha]}| W f(h)(\gamma_1 + i\gamma_2)|\psi_{[\theta\alpha]}\rangle/\sqrt{2}$. The effect appears when we use edge spins, hence

$$W = \sigma_1^z = \left(c_1 + c_1^\dagger\right) = \gamma_1 \tag{C5}$$

$$W = \sigma_N^z = \prod_{j<N}\left(1 - 2c_j^\dagger c_j\right)\left(c_N + c_N^\dagger\right)$$
$$= \mathbb{P}\left(c_N - c_N^\dagger\right) = i\mathbb{P}\gamma_2, \tag{C6}$$

where $\mathbb{P} = \prod_j^N \left(1 - 2c_j^\dagger c_j\right)$ is the parity operator. Eqs. C5-C6 show the operator W in Ising, Dirac and Majorana bases, respectively. If we work with the operator Eq. C5,

$$\langle\psi_{[\theta,\alpha]}| f(h)\gamma_1\left(\frac{\gamma_1+i\gamma_2}{\sqrt{2}}\right)|\psi_{[\theta,\alpha]}\rangle = \frac{2f(h)}{\sqrt{2}}, \tag{C7}$$

where we utilized $(\gamma_i)^2 = \mathbb{I}$ and $-i\gamma_1\gamma_2|\psi_{[\theta,\alpha]}\rangle = -|\psi_{[\theta,\alpha]}\rangle$ since $|\psi_{[\theta,\alpha]}\rangle$ is an odd-parity state. Similarly for Eq. C6,

$$if(h)\langle\psi_{[\theta,\alpha]}|\mathbb{P}\gamma_2\left(\frac{\gamma_1+i\gamma_2}{\sqrt{2}}\right)|\psi_{[\theta,\alpha]}\rangle = \frac{2f(h)}{\sqrt{2}}, \tag{C8}$$

where we additionally use $\mathbb{P}|\psi_{[\theta,\alpha]}\rangle = -|\psi_{[\theta,\alpha]}\rangle$. Given each degenerate subspace contributes equally, we write $C_\infty = 2f(h)^2$. A simple functional form of Eq. C4 is calculated as $C_\infty = 1 - h^2$ for $h < J$ and $C_\infty = 0$ for $h > J$ in Ref. [38]. We substitute this analytical result into Eq. (C4) and obtain $W_{[\theta,\gamma][\theta,\alpha]} = \sqrt{1-h^2}$ for $h > J$ in the topologically non-trivial phase. Hence we observe that the diagonal contribution of OTOC is a direct dynamical probe of topological order, giving a non-zero $F_{\rm ex}^{mj} = \left(1-h^2\right)^2$ in the non-trivial phase.

To demonstrate how $\bar{F}_{diag}$ of Ising model can match with Eq. (13) of non-interacting fermionic system whose calculation is purely based on Majorana zero-energy modes, we plot Fig. C1. Blue right-pointing triangles and orange left-pointing triangles show $\bar{F}_{diag}^{mj}$ numerically computed via Majorana zero-energy modes from BdG Hamiltonian for system sizes of $N = 14$ and $N = 100$, respectively. Note that $\bar{F}_{diag}^{is}$ of the Ising model (purple-squares) computed at $N = 14$ for a time interval of $tJ \sim 8$ matches well with F_{diag}^{mj} at the same size, implying that F_{diag}^{is} could be used to detect the presence/absence of Majorana zero-energy modes. The difference between $N = 14$ and $N = 100$ sizes of $\bar{F}_{diag}^{mj}$ shows how finite size effects show up near the transition point due to the divergent length scale associated with the quantum critical point. Additionally we compare $\bar{F}_{diag}^{mj}$ at $N = 100$ with the analytically derived result $\bar{F}_{\rm ex}^{mj}$ that is denoted by solid-orange line in Fig. C1 and observe that they match perfectly.

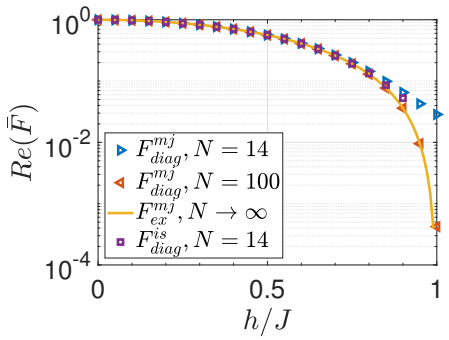

FIG. C1. Diagonal contribution in the Ising model and non-interacting fermionic model after dynamical decomposition is applied. Purple-circles show the diagonal contribution Eq. (12) at $N = 14$ in the Ising model (for a time interval $tJ = \frac{\pi}{4}10 \sim 7.85$), while the blue right-pointing triangles ($N = 14$) and red left-pointing triangles ($N = 100$) show Eq. (12) for $H_{\rm BdG}$ in non-interacting fermion system at infinite-time limit. The exact form is derived from the two-time correlators of Majorana fermions (solid-orange).

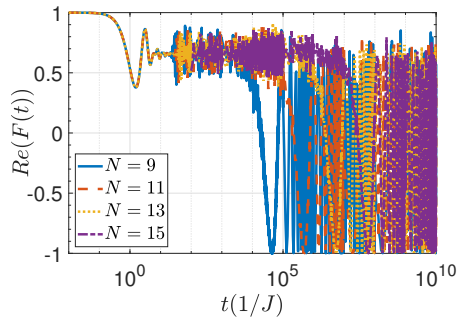

FIG. D1. Coherence time computation of the integrable Ising model deep in the non-trivial phase $h/J = 0.3$. The coherence times exhibit exponential increase with the system size which implies that pre-scrambling lasts indefinitely.

Appendix D: Further results on the Ising Model

Fig. D1 shows that the pre-scrambling time-scale scales with the system size in the Ising model. Hence, in the thermodynamic limit, pre-scrambling continues to survive, giving a finite OTOC saturation (time-average) $\bar{F} \neq 0$ at the infinite-time limit.

Fig. D2 shows the system-size scaling of fermionic OTOC time-average at the phase transition point that is also determined by OTOC itself. The scaling parameters of the phase transition point was already given in

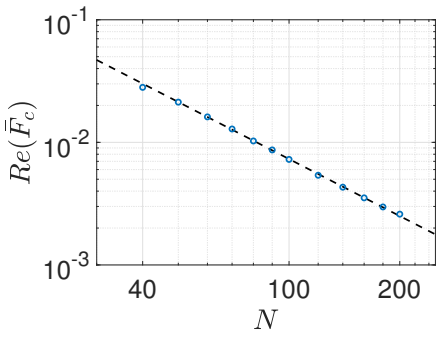

FIG. D2. The scaling of OTOC, F with the system size N at the transition point determined by the second derivative of the OTOC (see main text). The scaling parameters are: $F^{\infty} \sim N^{-1.5452} - 1$ with $R^2 = 0.9994$.

the main text. Here we provide the scaling parameters of the OTOC amplitude with respect to system size: $F^{\infty} \sim N^{-1.5452} - 1$, meaning the OTOC in thermodynamic limit should saturate at $F^{\infty} = -1$ in the transition point.

Finally we explicitly demonstrate the operator ansatz both satisfied and violated via the Ising model. For this, we plot the matrix elements $|V_{\beta\alpha}|^2$ for various β in the spectrum at different h values in Fig. D3. Note that $|\psi_\beta\rangle$ and $|\psi_\alpha\rangle$ in $|V_{\beta\alpha}|^2$ denote states sorted according to their energies. This notation should not be confused with $[\theta\alpha]$ notation in App. C where θ enumerates the degenerate manifolds.

The first two subfigures (a)-(b) are for an edge spin operator σ_1^z, whereas the rest (c)-(d) are for a bulk spin operator. We sample the ground state (a)-(c) and a state in the middle of the spectrum (b)-(d) in these subfigures. Deep in the topologically non-trivial phase, $h = 0.1$, we see that the operator ansatz is satisfied $|V_{[\theta\gamma][\theta\gamma']}|^2 \gg |V_{[\theta\gamma][\theta'\gamma']}|^2$ for an edge spin (blue-circles). For a bulk spin, the operator ansatz is valid only in the ground state subspace, hence it is actually $|V_{[1\gamma][1\gamma']}|^2 \gg |V_{[1\gamma][\theta'\gamma']}|^2$, the condition put forward by Ref. [19] for the dynamical detection of symmetry-breaking phase transitions via OTOCs. This is how the edge spins preserve the topological order in the OTOC throughout the spectrum, while the bulk spins can preserve only the symmetry-breaking order. Closer to the transition point, e.g. $h = 0.8$, the order $|V_{[\theta\gamma][\theta\gamma']}|^2$, expectantly, decreases while the off-diagonal matrix elements $|V_{[\theta\gamma][\theta'\gamma']}|^2$ grow, which is a signature of integrability at this special non-interacting limit. Hence the operator ansatz still in the topologically non-trivial phase breaks down, hence explaining how the OTOC saturation starts to be dominated by off-diagonal contributions (see Fig. 6b in the main text where $\bar{F} \neq \bar{F}_{diag}$ in the non-trivial phase). Note that this breakdown of the operator ansatz in the ordered phase does not happen for the bulk spin that is in its ground state, Fig. D3c. The red-squares at $h = 0.8$ exhibit $|V_{[1\gamma][1\gamma']}|^2 \gg |V_{[1\gamma][\theta'\gamma']}|^2$, though clearly getting

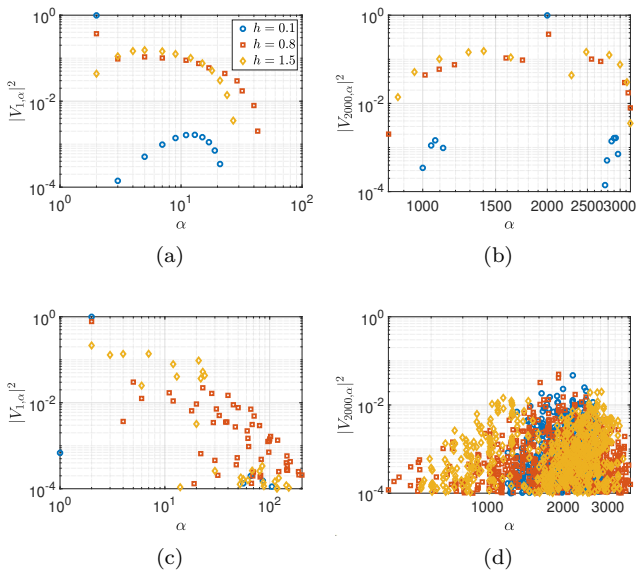

FIG. D3. The operator ansatz tested on the Ising model. Matrix elements $|V_{\beta\alpha}|^2$ are plotted for (a) $\beta = 1$ (b) $\beta = 2000$ with respect to α for an edge operator σ_1^z (open boundary); same β (c)-(d) for a bulk operator (periodic boundary) at a size $N = 12$. Blue-circles, red-squares and orange-diamonds stand for field strength $h/J = 0.1$, $h/J = 0.8$ and $h/J = 1.5$, respectively for all subfigures.

weaker as we approach the transition point. The operator ansatz in the topologically trivial phase, e.g. $h = 1.5$, $|V_{[\theta\gamma][\theta'\gamma']}|^2 \ll 1$, continues to fail (compare orange-diamonds with blue-circles in Figs. D3a-D3b). Eventually this causes a non-vanishing OTOC time-average $\bar{F} \neq 0$ in the trivial phase, even though this time-average has nothing to do with topological order (Sec. III B).

Appendix E: Further results on the non-integrable Ising models and XXZ model

The OTOC saturation of bulk spins in Figs. E1 behaves drastically different than of an edge spin: as we increase the system size, both $\bar{F}$ and F_{diag} approach to zero for all h, and hence gets even farther away from the transition point. Figs. E1a and E1b show the OTOC of bulk spins in the models with $\Delta/J = -0.1$ and $\Delta/J = -0.5$, respectively.

The coherence times of the edge spins at $\Delta/J = -2$ deep in the non-trivial phase (Fig. E2a) exhibit exponential increase with the system size in Fig. E2b up to an apparent odd-even effect. All different scaling samples collapse at around $\xi \sim 1$ for the exponent of the exponential scaling. While it is highly expected that this increase should slow down with bigger system sizes, based on our available data we cannot state that this behaviour is an example of pre-scrambling, instead it looks like a finite-size effect up until $N = 15$ system size. Hence it is not

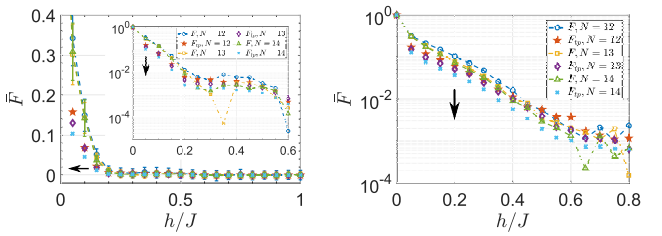

FIG. E1. Non-integrable transverse-field Ising model. OTOC time-average of bulk spins in (a) small integrability breaking term $\Delta/J = 0.1$ in linear and logarithmic (inset) scales. Red pentagrams, purple diamonds and light-blue crosses show F_{diag} whereas the blue circles, orange squares and green triangles show F for $N = 12$, $N = 13$ and $N = 14$, respectively. (b) The case of $\Delta/J = -0.5$ integrability breaking term. $\bar{F}$ and $\bar{F}_{diag}$ for $N = 12$ (blue-circles and red-pentagrams), $N = 13$ (orange-squares and purple-diamonds) and $N = 14$ (green-triangles and light-blue crosses). All curves have open boundary conditions and a time interval of $tJ \sim 800$.

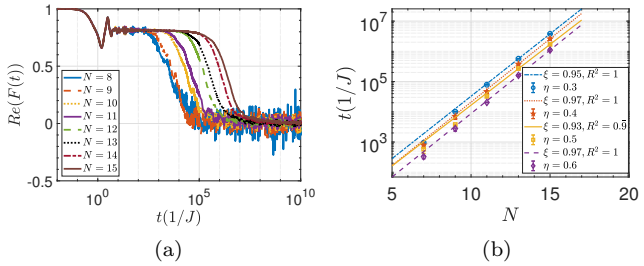

FIG. E2. (a) Coherence times of the edge spins based on OTOC at $\Delta/J = -2$, deep in the topologically non-trivial phase $h/J = 0.3$ and (b) the system-size scaling of the coherence times in (a). Note that different curves correspond to different threshold values η where we look for the times that provide $F(t) = \eta$. ξ is the exponent in the exponential scaling and all of them are around $\xi \sim 1$.

always easy to extract a curve collapse to demonstrate pre-scrambling in systems with small sizes.

Fig. E3 demonstrates the dependence of a dynamic phase diagram on the interval of time averaging. The data is for the weakly-interacting generic model. The result with blue-circles that is computed in a short time interval of $tJ = 10$ converges to the OTOC of non-interacting limit, while increasing the averaging time from $tJ = 10$ to later times causes the phase diagram to change significantly. Hence in the short-time limit, the coherence times of the edge spins are significantly contributed not only by the diagonal elements, but also the off-diagonal elements of the edge operator. This additional contribution, that is specific to OTOC, in fact survives until very long times, e.g. $t \gtrsim 2 \times 10^3$ (Fig. 7b in main text). However, farther away from the non-interacting limit the off-diagonal contributions vanish faster, whereas the diagonal contribution remains for longer times.

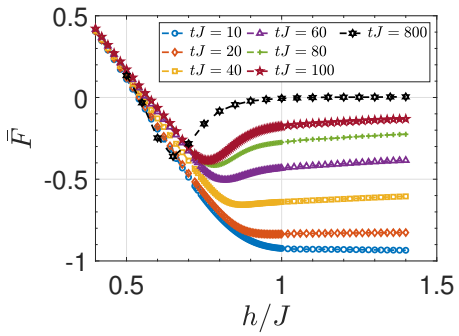

FIG. E3. Demonstration of the time-dependence of the phase diagram for the model with $\Delta/J = 0.1$ at $N = 14$ system size. Blue circles, orange diamonds, yellow squares, purple triangles, green pluses, red pentagrams and black hexagrams stand for $tJ = 10, 20, 40, 60, 80, 100, 800$, respectively.

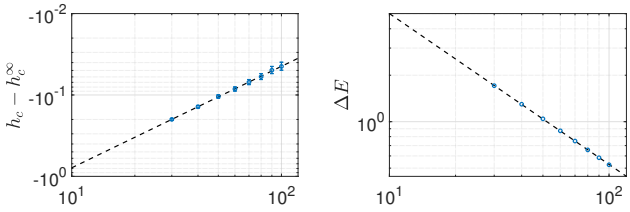

FIG. E4. The scaling parameters for the ground state phase transition of the model with $\Delta/J = -2$, calculated via DMRG. (a) The system-size scaling of the critical point, giving $h_c^\infty = 3.7746$ in the thermodynamic limit. (b) The system-size scaling of the energy gap, giving an exponent of ~ -1 and showing that the gap closes in the thermodynamic limit.

We provide DMRG results to mark the ground state phase transition point in the model with $\Delta/J = -2$ via minimizing the energy gap at the transition point. The scaling parameters for the transition point read $h_c \sim N^{-1.2467} + 3.7746$ where the transition point in the thermodynamic limit is found $h_c^\infty = 3.7746$ with $R^2 = 0.9997$. The scaling parameters for the energy gap read $\Delta E \sim N^{-0.9775}$ with $R^2 = 0.9999$. So the system-size scaling exponent for the energy gap is close to -1. See Figs. E4 for the scaling figures.

Appendix F: Further results on the XXZ model

Fig. F1 shows long-time dynamics of OTOC in the gapless phase of the XXZ model and how the time-average of this signal scales with the system size. We see the scaling has a form of $Re(\bar{F}) \propto N^{-\xi}$ where $\xi \sim 0.9$. Hence in the thermodynamic limit we expect $\bar{F} \to 0$ in the gapless

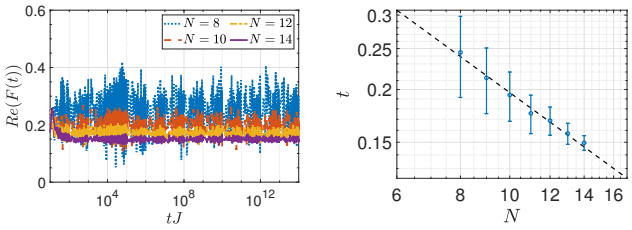

(a) (b)

FIG. F1. (a) The saturation value for long times and different system sizes ($N = 8$ to $N = 14$) are plotted for the gapless phase of the XXZ model. (b) The system size scaling of the saturation value where the error bars show the extend of the oscillations around the average of the signals in (a). The scaling has a form of $Re(\bar{F}) \propto N^{-\xi}$ where $\xi \sim 0.9$.

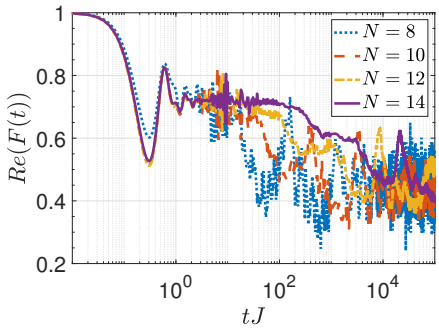

FIG. F2. The coherence times of pre-scrambling in the gapped phase of the XXZ model, $J_z/J = 5$ for different system sizes. The exponential increase in the pre-scrambling time intervals with the system size suggests that the scrambling seen is a finite-size effect.

phase.

Fig. F2 shows pre-scrambling time scales exponentially increase with the system size, a similar figure to Fig. 7d in the main text, however much closer to the transition boundary. The exponential increase in system size implies that the scrambling is a finite-size effect, hence in thermodynamic limit, pre-scrambling should persist, giving $\bar{F} \neq 0$ in the topologically non-trivial gapped phase.

[1] Y. Sekino and L. Susskind, "Fast scramblers," Journal of High Energy Physics **10**, 065 (2008), arXiv:0808.2096 [hep-th].

[2] N. Lashkari, D. Stanford, M. Hastings, T. Osborne, and P. Hayden, "Towards the fast scrambling conjecture," Journal of High Energy Physics **4**, 22 (2013), arXiv:1111.6580 [hep-th].

[3] B. Swingle and D. Chowdhury, "Slow scrambling in disordered quantum systems," Phys. Rev. B **95**, 060201 (2017), arXiv:1608.03280 [cond-mat.str-el].

[4] K. Hashimoto, K. Murata, and R. Yoshii, "Out-of-time-order correlators in quantum mechanics," Journal of High Energy Physics **10**, 138 (2017), arXiv:1703.09435 [hep-th].

[5] Martin Grttner, Justin Bohnet, Arghavan Safavi-Naini, Michael L. Wall, John J. Bollinger, and Ana Rey, "Measuring out-of-time-order correlations and multiple quantum spectra in a trapped ion quantum magnet," *Nature Physics*, **13** (2016).

[6] Stephen H. Shenker and Douglas Stanford, "Black holes and the butterfly effect," Journal of High Energy Physics **2014**, 67 (2014), arXiv:1306.0622 [hep-th].

[7] Yasuhiro Sekino and L. Susskind, "Fast scramblers," Journal of High Energy Physics **2008**, 065 (2008).

[8] Juan Maldacena, Stephen H. Shenker, and Douglas Stanford, "A bound on chaos," Journal of High Energy Physics **2016**, 106 (2016).

[9] Jun Li, Ruihua Fan, Hengyan Wang, Bingtian Ye, Bei Zeng, Hui Zhai, Xinhua Peng, and Jiangfeng Du, "Measuring out-of-time-order correlators on a nuclear magnetic resonance quantum simulator," Phys. Rev. X **7**, 031011 (2017).

[10] Xiao Chen, Tianci Zhou, David A. Huse, and Eduardo Fradkin, "Out-of-time-order correlations in many-body localized and thermal phases," Annalen der Physik **529**, 1600332.

[11] A. Bohrdt, C. B. Mendl, M. Endres, and M. Knap, "Scrambling and thermalization in a diffusive quantum many-body system," New Journal of Physics **19**, 063001 (2017), arXiv:1612.02434 [cond-mat.quant-gas].

[12] Shenglong Xu and Brian Swingle, "Accessing scrambling using matrix product operators," arXiv e-prints , arXiv:1802.00801 (2018), arXiv:1802.00801 [quant-ph].

[13] Yichen Huang, Yong-Liang Zhang, and Xie Chen, "Out-of-time-ordered correlators in many-body localized systems," Annalen der Physik **529**, 1600318 (2017).

[14] Rong-Qiang He and Zhong-Yi Lu, "Characterizing many-body localization by out-of-time-ordered correlation," Physical Review B **95**, 054201 (2017), arXiv:1608.03586 [cond-mat.dis-nn].

[15] Ceren B. Dağ and L.-M. Duan, "Detection of out-of-time-order correlators and information scrambling in cold atoms: Ladder-XX model," Phys. Rev. A **99**, 052322 (2019).

[16] Cheng-Ju Lin and Olexei I. Motrunich, "Out-of-time-ordered correlators in a quantum ising chain," Phys. Rev. B **97**, 144304 (2018).

[17] Eiki Iyoda and Takahiro Sagawa, "Scrambling of quantum information in quantum many-body systems," Phys. Rev. A **97**, 042330 (2018).

[18] Huitao Shen, Pengfei Zhang, Ruihua Fan, and Hui Zhai, "Out-of-time-order correlation at a quantum phase transition," Phys. Rev. B **96**, 054503 (2017).

[19] Ceren B. Dağ, Kai Sun, and L. M. Duan, "Detection of quantum phases via out-of-time-order correlators," arXiv e-prints (2019), arXiv:1902.05041 [quant-ph].

[20] Markus Heyl, Frank Pollmann, and Balázs Dóra, "Detecting equilibrium and dynamical quantum phase transitions in ising chains via out-of-time-ordered correlators," Phys. Rev. Lett. **121**, 016801 (2018).

[21] David J. Luitz and Yevgeny Bar Lev, "Information propagation in isolated quantum systems," Phys. Rev. B **96**, 020406 (2017).

[22] Sheldon Goldstein, Joel L. Lebowitz, Roderich Tumulka, and Nino Zanghì, "Canonical typicality," Phys. Rev. Lett. **96**, 050403 (2006).

[23] Sandu Popescu, Anthony J Short, and Andreas Winter, "Entanglement and the foundations of statistical mechanics," Nature Physics **2**, 754 (2006).

[24] Peter Reimann, "Typicality for generalized microcanonical ensembles," Phys. Rev. Lett. **99**, 160404 (2007).

[25] Sho Sugiura and Akira Shimizu, "Thermal pure quantum states at finite temperature," Phys. Rev. Lett. **108**, 240401 (2012).

[26] David J. Luitz and Yevgeny Bar Lev, "The ergodic side of the many-body localization transition," Annalen der Physik **529**, 1600350 (2017), arXiv:1610.08993 [cond-mat.dis-nn].

[27] Brian Swingle, "Unscrambling the physics of out-of-time-order correlators," Nature Phys. **14**, 988–990 (2018).

[28] A. Yu Kitaev, "Unpaired Majorana fermions in quantum wires," Physics Uspekhi **44**, 131 (2001), arXiv:cond-mat/0010440 [cond-mat.mes-hall].

[29] Xiao-Gang Wen, "Colloquium: Zoo of quantum-topological phases of matter," Rev. Mod. Phys. **89**, 041004 (2017).

[30] J. Berges, Sz. Borsányi, and C. Wetterich, "Prethermalization," Phys. Rev. Lett. **93**, 142002 (2004).

[31] Takashi Mori, Tatsuhiko N. Ikeda, Eriko Kaminishi, and Masahito Ueda, "Thermalization and prethermalization in isolated quantum systems: a theoretical overview," Journal of Physics B Atomic Molecular Physics **51**, 112001 (2018), arXiv:1712.08790 [cond-mat.stat-mech].

[32] Ruihua Fan, Pengfei Zhang, Huitao Shen, and Hui Zhai, "Out-of-time-order correlation for many-body localization," Science Bulletin **62**, 707 – 711 (2017).

[33] Jiahui Bao and Cheng-Yong Zhang, "Out-of-Time-Order Correlators in One-Dimensional XY model," arXiv e-prints , arXiv:1901.09327 (2019), arXiv:1901.09327 [cond-mat.stat-mech].

[34] S. Sachdev, *Quantum Phase Transitions* (Cambridge University Press, 2001).

[35] Jack Kemp, Norman Y. Yao, Christopher R. Laumann, and Paul Fendley, "Long coherence times for edge spins," Journal of Statistical Mechanics: Theory and Experiment **6**, 063105 (2017), arXiv:1701.00797 [cond-mat.stat-mech].

[36] Dominic V. Else, Paul Fendley, Jack Kemp, and Chetan Nayak, "Prethermal strong zero modes and topological qubits," Phys. Rev. X **7**, 041062 (2017).

[37] Sthitadhi Roy, Roderich Moessner, and Arnab Das, "Locating topological phase transitions using nonequilibrium signatures in local bulk observables," Phys. Rev. B **95**, 041105 (2017).

[38] F. J. Gómez-Ruiz, J. J. Mendoza-Arenas, F. J. Rodríguez, C. Tejedor, and L. Quiroga, "Universal two-time correlations, out-of-time-ordered correlators, and leggett-garg inequality violation by edge majorana fermion qubits," Phys. Rev. B **97**, 235134 (2018).

[39] Yucheng Wang, "Detecting topological phases via survival probabilities of edge majorana fermions," Phys. Rev. E **98**, 042128 (2018).

[40] M. D. Caio, N. R. Cooper, and M. J. Bhaseen, "Quantum quenches in chern insulators," Phys. Rev. Lett. **115**, 236403 (2015).

[41] Jinlong Yu, "Phase vortices of the quenched haldane model," Phys. Rev. A **96**, 023601 (2017).

[42] Ying Hu, Peter Zoller, and Jan Carl Budich, "Dynamical buildup of a quantized hall response from nontopological states," Phys. Rev. Lett. **117**, 126803 (2016).

[43] N. Fläschner, D. Vogel, M. Tarnowski, B. S. Rem, D.-S. Lühmann, M. Heyl, J. C. Budich, L. Mathey, K. Sengstock, and C. Weitenberg, "Observation of dynamical vortices after quenches in a system with topology," Nature Physics **14**, 265–268 (2018).

[44] Luca D'Alessio and Marcos Rigol, "Dynamical preparation of Floquet Chern insulators," Nature Communications **6**, 8336 (2015), arXiv:1409.6319 [cond-mat.quant-gas].

[45] Max McGinley and Nigel R. Cooper, "Classification of topological insulators and superconductors out of equilibrium," Phys. Rev. B **99**, 075148 (2019).

[46] Alexei Kitaev, "Periodic table for topological insulators and superconductors," AIP Conference Proceedings **1134**, 22–30 (2009).

[47] M. Heyl, A. Polkovnikov, and S. Kehrein, "Dynamical Quantum Phase Transitions in the Transverse-Field Ising Model," Phys. Rev. Lett. **110**, 135704 (2013), arXiv:1206.2505 [cond-mat.stat-mech].

[48] Jan Carl Budich and Markus Heyl, "Dynamical topological order parameters far from equilibrium," Phys. Rev. B **93**, 085416 (2016).

[49] Markus Schmitt and Stefan Kehrein, "Dynamical quantum phase transitions in the kitaev honeycomb model," Phys. Rev. B **92**, 075114 (2015).

[50] Fabio Franchini, *An Introduction to Integrable Techniques for One-Dimensional Quantum Systems, Lecture Notes in Physics, Volume 940. ISBN 978-3-319-48486-0.* (2017).

[51] Yichen Huang, Fernando G. S. L. Brandão, and Yong-Liang Zhang, "Finite-size scaling of out-of-time-ordered correlators at late times," Phys. Rev. Lett. **123**, 010601 (2019).

[52] M. Rigol, V. Dunjko, and M. Olshanii, "Thermalization and its mechanism for generic isolated quantum systems," Nature (London) **452**, 854–858 (2008), arXiv:0708.1324 [cond-mat.stat-mech].

[53] Luca D'Alessio, Yariv Kafri, Anatoli Polkovnikov, and Marcos Rigol, "From quantum chaos and eigenstate thermalization to statistical mechanics and thermodynamics," Advances in Physics **65**, 239–362 (2016), arXiv:1509.06411 [cond-mat.stat-mech].

[54] Christian Gogolin and Jens Eisert, "Equilibration, thermalisation, and the emergence of statistical mechanics in closed quantum systems," Reports on Progress in Physics **79**, 056001 (2016), arXiv:1503.07538 [quant-ph].

[55] Paraj Titum, Joseph T. Iosue, James R. Garrison, Alexey V. Gorshkov, and Zhe-Xuan Gong, "Prob-

ing ground-state phase transitions through quench dynamics," arXiv e-prints , arXiv:1809.06377 (2018), arXiv:1809.06377 [quant-ph].

[56] Zheng-Hang Sun, Jia-Qi Cai, Qi-Cheng Tang, Yong Hu, and Heng Fan, "Out-of-time-order correlators and quantum phase transitions in the Rabi and Dicke model," arXiv e-prints , arXiv:1811.11191 (2018), arXiv:1811.11191 [quant-ph].

[57] Alexei Kitaev and John Preskill, "Topological entanglement entropy," Phys. Rev. Lett. **96**, 110404 (2006).

[58] Michael Levin and Xiao-Gang Wen, "Detecting topological order in a ground state wave function," Phys. Rev. Lett. **96**, 110405 (2006).

[59] Hong-Chen Jiang, Zhenghan Wang, and Leon Balents, "Identifying topological order by entanglement entropy," Nature Physics **8**, 902–905 (2012), arXiv:1205.4289 [cond-mat.str-el].

[60] C. W. von Keyserlingk, Tibor Rakovszky, Frank Pollmann, and S. L. Sondhi, "Operator hydrodynamics, otocs, and entanglement growth in systems without conservation laws," Phys. Rev. X **8**, 021013 (2018).

[61] ITensor Library (version 2.0.11) http://itensor.org.

[62] M. Srednicki, "Thermal Fluctuations in Quantized Chaotic Systems," in *eprint arXiv:chao-dyn/9511001* (1995).

[63] M. Srednicki, "The approach to thermal equilibrium in quantized chaotic systems," Journal of Physics A Mathematical General **32**, 1163–1175 (1999), cond-mat/9809360.